

paths starting with widely different initial conditions. This strongly suggests that this state of motion is stable. Probably it is unique for ordinary launchings. It is plausible that each boomerang has a characteristic final state of motion. For instance, flight path calculations made for boomerang 195.1 (level 3) yielded a final state characterized by the values:

$$f = 9.2 \text{ rev/s}, V = 13.5 \text{ m/s}, U = 0.78, \Psi = 9.2^\circ, \theta = 61^\circ, \psi = 161^\circ,$$

$$\phi = 18.4, \Delta Z = 22.1 \text{ m}, \Delta t = 4.7 \text{ sec.}$$

Necessary conditions for a boomerang's final state of motion are:

$$\dot{V} = 0, \dot{\omega}_z = 0, \dot{\Psi} = 0, \dot{\theta} = 0, \dot{\psi} = 0. \quad (28.1)$$

These are 5 equations for the 5 unknowns  $V, \omega_z, \Psi, \theta, \psi$ . The equations can be solved by putting the right-handed sides of the equations (4.8) and (4.9) equal to zero. If (28.1) is satisfied,  $\dot{\phi} = \text{constant}$  according to (4.9), and  $\dot{Z} = \text{constant}$  while  $\dot{X}$  and  $\dot{Y}$  vary harmonically with  $\phi$  according to (4.10). We shall not discuss the conditions for the existence, the stability, or the uniqueness of a boomerang's final state of motion.

In the boomerang flight presented in this section, the path curves counterclockwise ( $\phi$  increases) until  $t = 6.2 \text{ sec.}$  ( $Z = 4.6 \text{ m}$ ); after this  $\phi$  decreases and the path curves clockwise. In other cases this reversal may occur at an earlier or at a later instant. This phenomenon can often be observed in real boomerang flights. Sometimes a boomerang may be well on its way to its final state of motion before it hits the ground. Curiously, the first counterclockwise loop, so characteristic for the flight of a right-handed boomerang, may be considered as merely a transient form of motion, soon leading up to the boomerang's final state.

In the final state of motion discussed above, the gravitational force plays a crucial role. What would happen in the absence of gravity? In the following we shall suppose that  $g = 0$ , that the air is homogeneous (with density  $\mu = 1.20 \text{ kg/m}^3$ ), and that there is no wind. The equations of motion (4.8), (4.9), (4.10) now are modified in an important aspect: for a given boomerang  $\dot{V}, \dot{\omega}_z$  and  $\dot{\Psi}$  depend only on the aerodynamic forces, and hence (in our model) only on  $V, \omega_z$  and  $\Psi$ . The shape of the boomerang's flight path is independent of  $\theta_0, \phi_0, \psi_0, X_0, Y_0, Z_0$ . The path in

$(\Psi, U)$ -space traversed by the boomerang depends only on  $\Psi_0$  and  $U_0$ , while  $V_0$  (or  $f_0$ ) determines the velocity at which this path is traversed.

A necessary condition for  $\Psi$  being stationary is given by (22.1), and for  $U$  being stationary by (22.2). The restriction  $\vartheta = \frac{1}{2}\pi$ ,  $\psi = 0$  is not relevant now because gravity is absent. The boomerang will travel to a point with  $\dot{\Psi} = 0$ ,  $\dot{U} = 0$ :  $(\Psi^*, U^*)$  (under conditions not investigated by us). Because the boomerang continually loses kinetic energy  $V$  and  $\omega_z$  (or  $f$ ) decrease. Since  $\dot{V}(\cdot) - V^2$ ,  $V$  decreases inversely with time, and the boomerang's path length increases logarithmically with time. The boomerang ends up moving, slower and slower, along a helical path, away to infinity.

A gravitationless flight for boomerang 101.1 was computed with the initial conditions:  $f_0 = 10$  rev/s,  $V_0 = 25$  m/s,  $\Psi_0 = 0^\circ$ . This boomerang's final motion is characterized by:

$$\Psi^* = 2.0^\circ, U^* = 0.86$$

and the helical path by:

$$\phi = 34 \text{ m}, \Delta R = 31 \text{ m}, \Delta P = 112 \text{ m}, \Delta n = 70$$

where  $\phi$  is the diameter of the helix,  $\Delta R$  is the difference in the boomerang's position,  $\Delta P$  the path length and  $\Delta n$  the number of revolutions between two points one turn of the helix apart. The helix is traversed clockwise as seen from the point of launching. The direction of the helix' axis depends on  $\vartheta_0$ ,  $\phi_0$  and  $\psi_0$ . The helical motion begins rather soon after the start: already at  $t = 7$  sec. we have  $\Psi = 2.0^\circ$ ,  $U = 0.86$ . At  $t = 18.3$  sec. the boomerang has completed 100 spin revolutions and  $f = 2.9$  rev/s,  $V = 4.7$  m/s. At  $t = 94.1$  sec. 200 revolutions are completed and  $f = 0.7$  rev/s,  $V = 1.1$  m/s.

The relative simple shape of the flight path in the gravitationless case is due to the fact that the motion proceeds at constant values for  $\Psi$  and  $U$ . In the presence of gravity there is no fixed equilibrium point  $(\Psi^*, U^*)$ , and the boomerang moves about in the  $(\Psi, U)$ -plane. Much of the charm of real boomerang flights originates from the interplay of aerodynamic and gravitational forces.

§29 Wind.

In the practice of boomerang throwing the influence of wind on the boomerang's flight can be an important factor. Even a very light breeze of 1 m/s may significantly alter the shape of a flight path. In the absence of wind it does not matter whether the boomerang is thrown to the south or to the north; the flight path will have the same shape. As soon as there is wind, the direction in which the boomerang is launched does matter, and the angle  $\varphi_0$  may be a very important parameter indeed. If the wind is too strong, a boomerang's performance may be spoilt, the boomerang is taken with the wind and invariably lands at a considerable distance downwind. On the other hand, a moderate breeze may assist a boomerang in coming back. After carrying out a few trial throws in which the angle  $\varphi_0$  is varied, the boomerang thrower may obtain perfect return flights. This is particularly pleasing if the boomerang in case is incapable of returning well under windless conditions. Usually the optimum launching conditions are such that  $\beta - \varphi_0 \approx 45^\circ$  ( $\beta$  determines the wind's direction, see §8).

Two such cases are shown in fig. 29.1 and fig. 29.2. The 4 flight paths are computed for boomerang 245.1 (level 3), which is associated with boomerang L5, see §18. For the flights of fig. 29.1 the initial conditions are:

$$f_0 = 10 \text{ rev/s}, V_0 = 25 \text{ m/s}, \psi_0 = 0,$$

$$\theta_0 = 80^\circ, \varphi_0 = 0^\circ, \psi_0 = -20^\circ,$$

$$X_0 = 0 \text{ m}, Y_0 = 0 \text{ m}, Z_0 = 1.8 \text{ m},$$

a) no wind,

$$\text{b) } \beta = 45^\circ, W_0 = 1.3 \text{ m/s}, W_1 = 0.6 \text{ m/s/10 m}.$$

In the flights of fig. 29.2 the initial conditions are the same, except that  $\theta_0 = 70^\circ, \psi_0 = -30^\circ$ .

	wind	t	P	n	D	Z <sub>2</sub>	D <sub>2</sub>	D <sub>1</sub>	f <sub>2</sub>	f <sub>1</sub>	V' <sub>1</sub>	ψ' <sub>2</sub>	U' <sub>1</sub>
29.1	no	10.1	112.6	98.5	17.6	13.4	44.1	15.7	10.6	9.0	2.0	80.9	.10
	yes	9.9	121.9	94.6	1.2	15.9	41.1	0.9	10.3	8.9	2.9	80.1	.09
29.2	no	12.2	114.2	122.1	24.1	16.1	39.2	20.5	11.1	9.0	2.4	64.8	.11
	yes	13.3	122.0	134.0	4.3	18.0	34.0	2.6	11.3	9.0	2.1	52.8	.13

table 29.1. Some values for the flights of fig. 29.1 and 29.2.

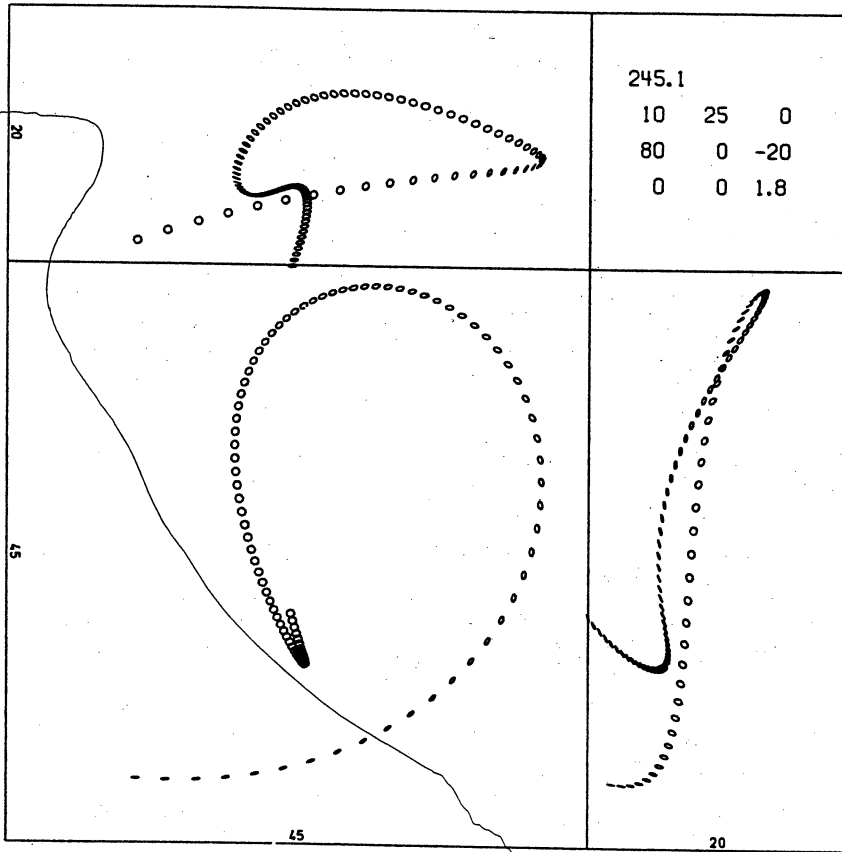


fig. 29.1a

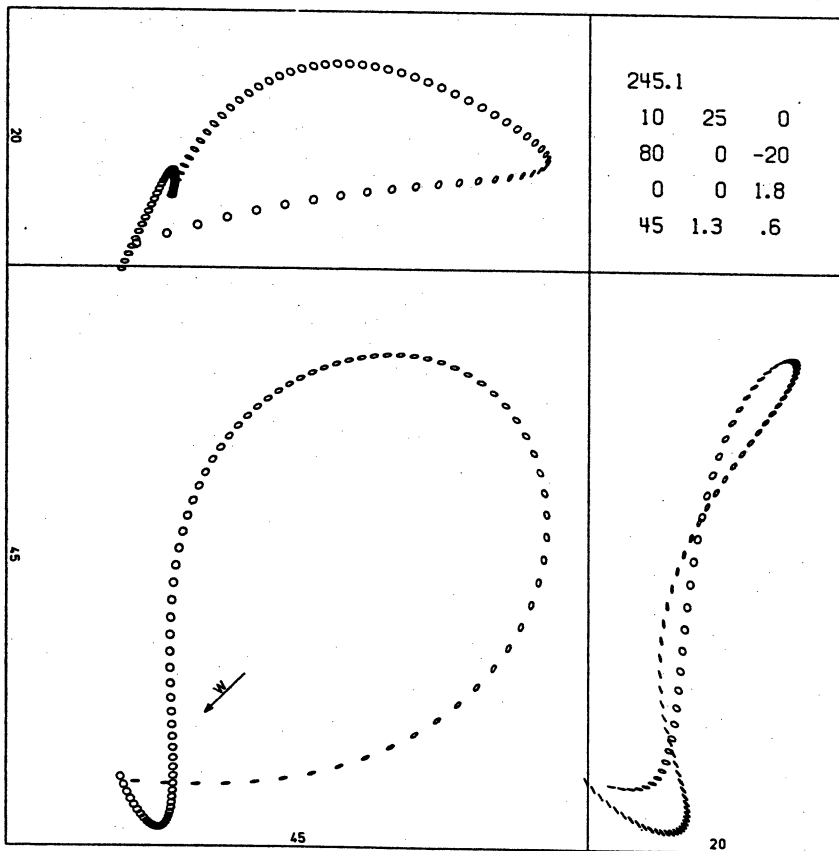


fig. 29.1b

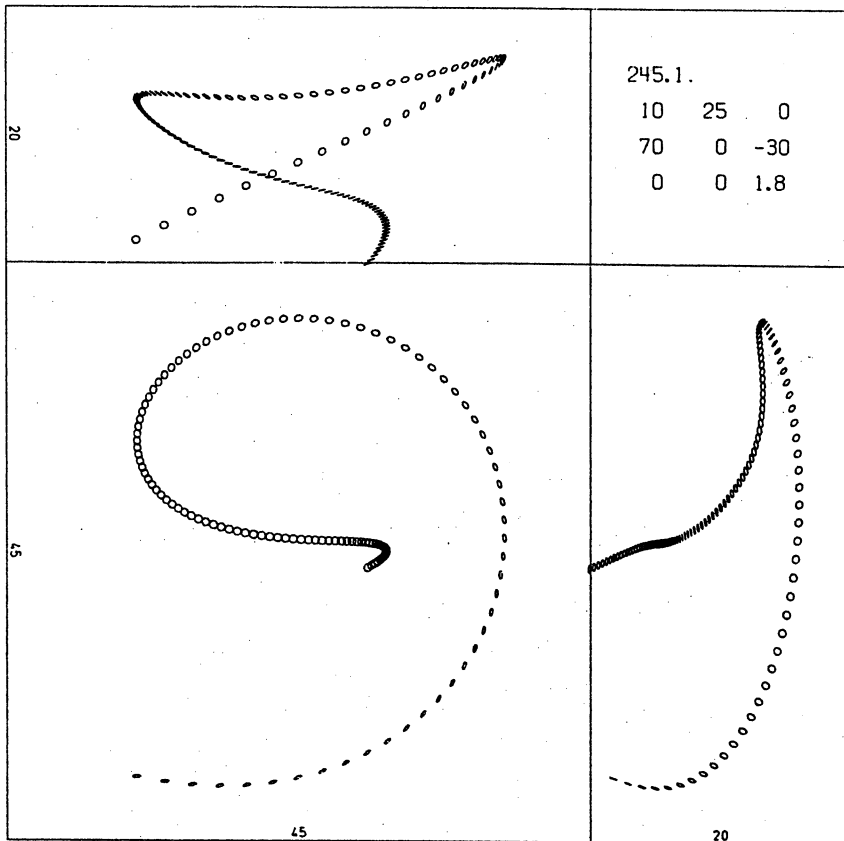


fig. 29.2a

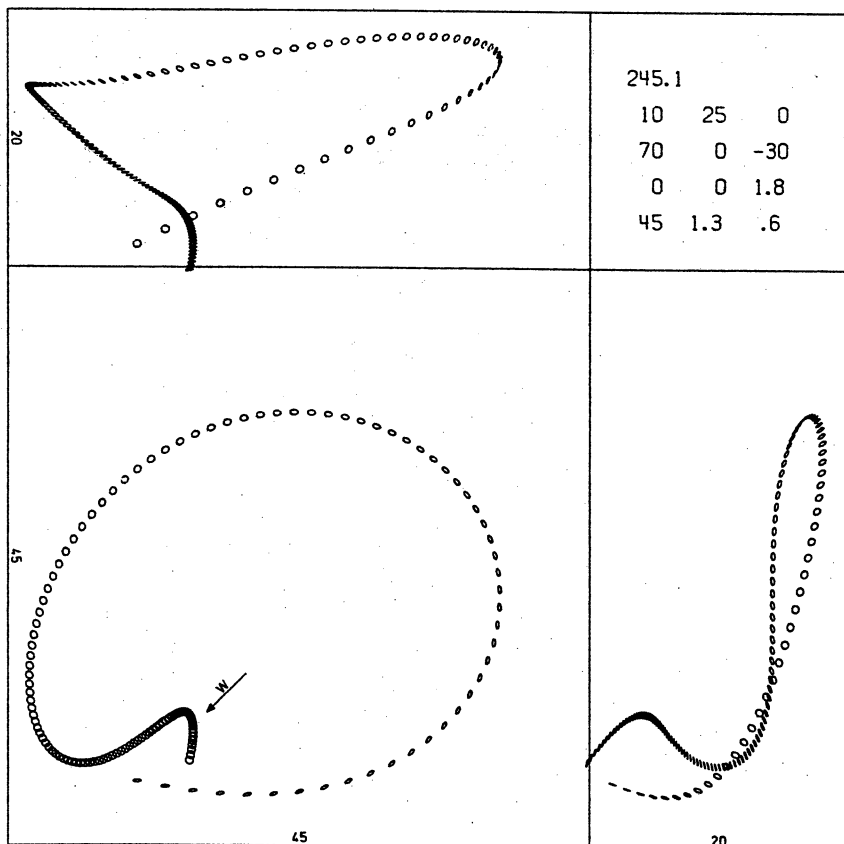


fig. 29.2b

Some values for these 4 flights are listed in table 29.1. In these examples the light breeze helps the boomerang to return beautifully. It is rather unfortunate that the field experiments with boomerang L5 (see §18) did not produce level 1 flight paths suitable for determining the influence of wind.

The main influence of the wind on a boomerang's flight can be explained as follows. Suppose the wind velocity field is constant and homogeneous ( $W_1 = 0$ ). Use a coordinate system ( $X', Y', Z'$ ) moving with the air. In this inertial frame the air is motionless. However, the initial conditions for the boomerang's flight are modified:  $V_0$ ,  $\Psi_0$  and  $U_0$  have to be replaced by  $V'_0$ ,  $\Psi'_0$  and  $U'_0$  according to §8. For instance, if a boomerang is launched directly into the wind,  $V'_0 > V_0$  and  $U'_0 > U_0$ . In the ( $X', Y', Z'$ )-system the boomerang traverses an ordinary flight path, starting with the modified initial conditions. This trajectory can be transformed back to the old ( $X, Y, Z$ )-system according to:

$$\left. \begin{aligned} X(t) &= X'(t) + tW\cos\beta \\ Y(t) &= Y'(t) + tW\sin\beta \\ Z(t) &= Z'(t) \end{aligned} \right\} (29.1)$$

where  $W$  is the constant wind speed. If  $W$  is very small, the modification of the initial conditions has little influence, and the main effect of the wind is that the velocity of the air is added to the velocity of the boomerang. If the flight lasts for a time  $T$ , the landing point is shifted downwind over a distance  $\approx WT$ . In reality the wind speed varies in space and time, but the above line of reasoning usually is qualitatively valid.

In fig. 29.3a through h flight paths are shown for boomerang 101.1 (level 2), which are computed with the initial conditions:

$$\begin{aligned} f_0 &= 10 \text{ rev/s}, V_0 = 25 \text{ m/s}, \Psi_0 = 0^\circ, \\ \theta_0 &= 80^\circ, \varphi_0 = 0^\circ, \psi_0 = -10^\circ, \\ X_0 &= 0 \text{ m}, Y_0 = 0 \text{ m}, Z_0 = 1.8 \text{ m}, \\ \beta &= \text{variable}, W_0 = 2 \text{ m/s}, W_1 = 1 \text{ m/s/10 m.} \end{aligned}$$

The values chosen for  $\beta$  are respectively:  $0^\circ, 45^\circ, 90^\circ, 135^\circ, 180^\circ, 225^\circ, 270^\circ, 315^\circ$ .

$\beta$	$V'_0$	$U'_0$	$\Psi'_0$	D	$Z_2$
none	25.0	1.34	0.0	7.7	9.9
0°	27.1	1.45	0.0	27.1	13.0
45°	26.5	1.42	-3.3	20.0	12.6
90°	25.0	1.34	-4.9	14.6	10.6
135°	23.5	1.25	-3.7	17.9	8.2
180°	22.9	1.22	0.0	22.1	6.8
225°	23.6	1.26	3.7	25.0	7.4
270°	25.2	1.34	4.9	28.1	9.4
315°	26.6	1.42	3.3	28.8	11.7

table 29.2. Some values for the flights of fig. 29.3.

The wind speed at ground level  $Z=0$  is 2 m/s, at  $Z=10$  m: 3 m/s and at the launching point: 2.18 m/s. Values for the "modified initial conditions",  $V'_0$ ,  $U'_0$ ,  $\Psi'_0$  for these flights are listed in table 29.2 together with values for the maximum elevation  $Z_2$  and the distance of the landing point D. In all 8 cases the average wind speed of about 2.5 m/s encountered by the boomerang spoils the return performance. Two main effects are visible: 1<sup>o</sup> the boomerang is transported downwind, and 2<sup>o</sup> the maximum height  $Z_2$  increases with increasing values of  $\cos(\beta-\varphi)$ , varying between 6.8 m for the throw downwind to 12.6 m for the throw upwind.

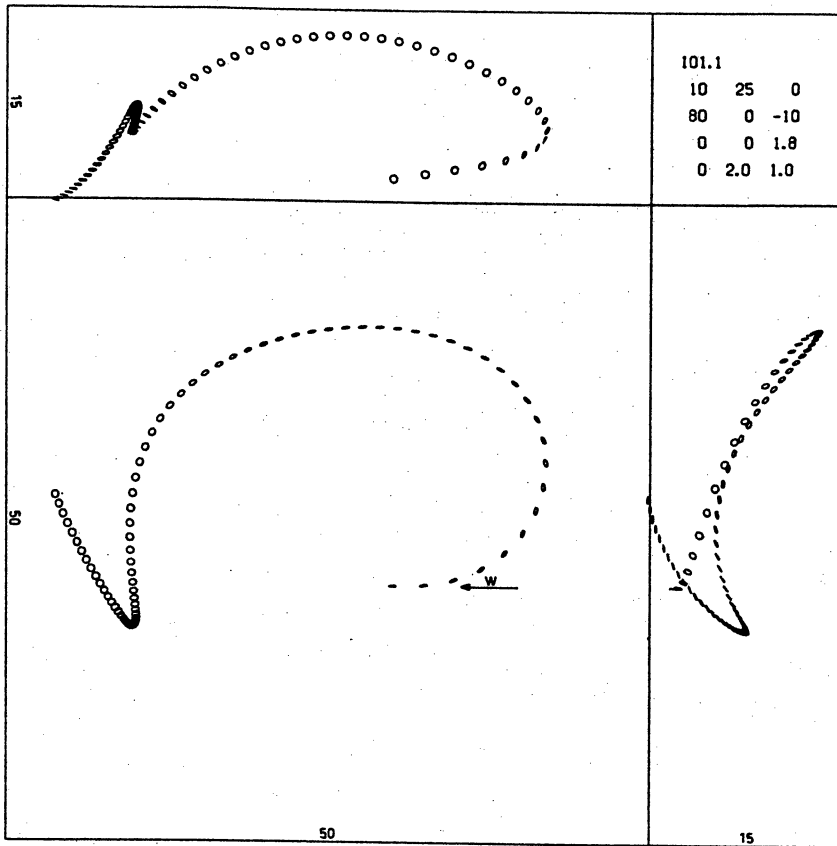


fig. 29.3a

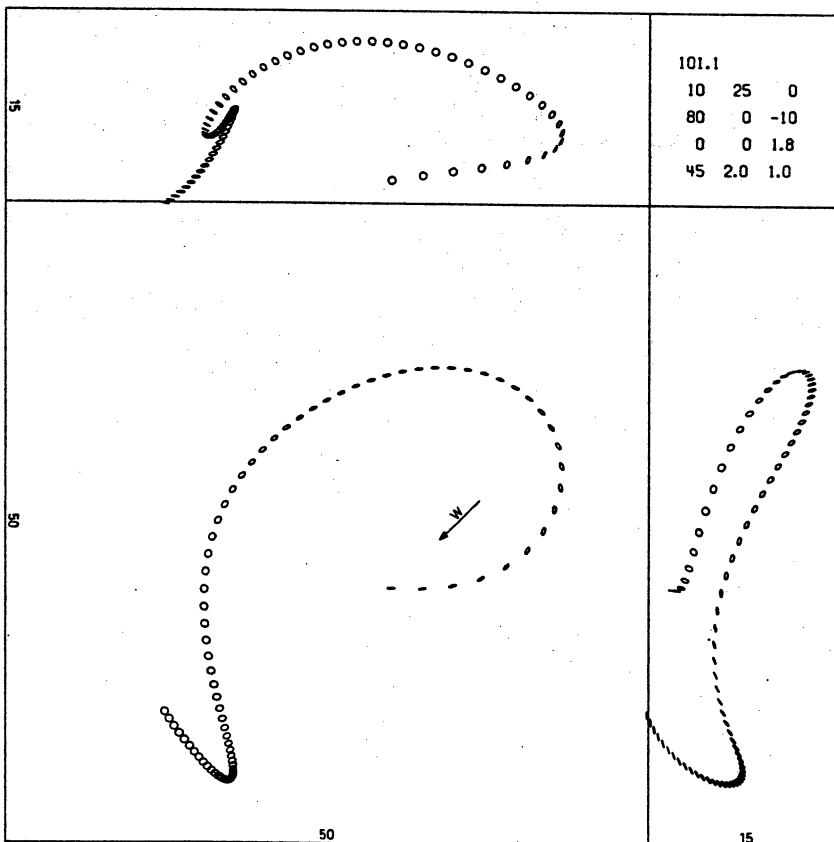


fig. 29.3b

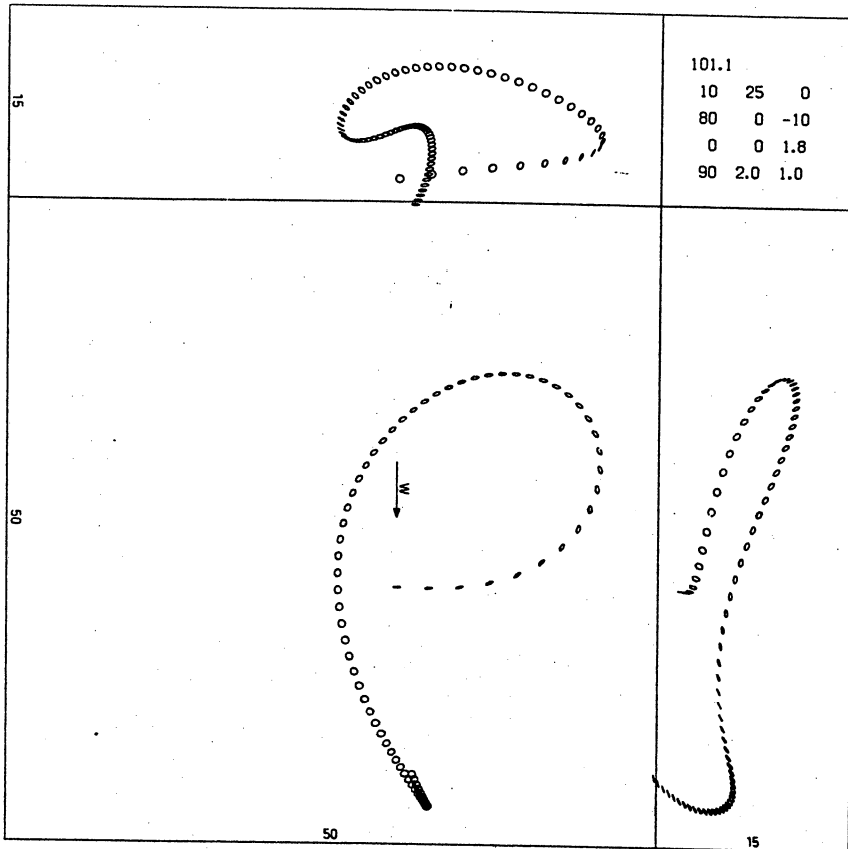


fig. 29.3c

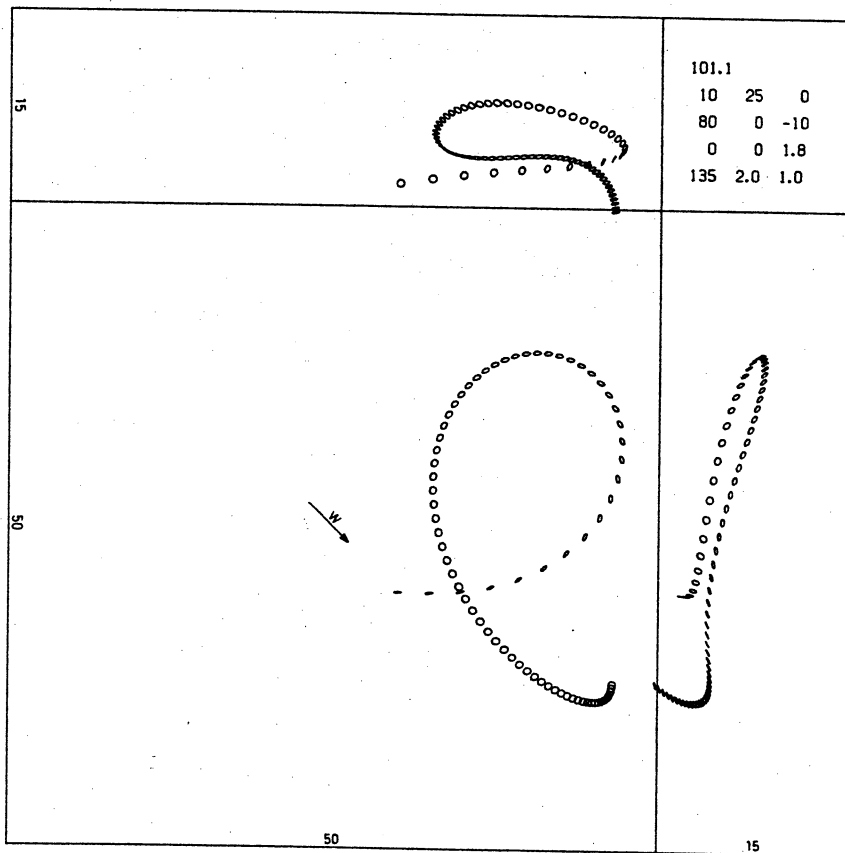


fig. 29.3d

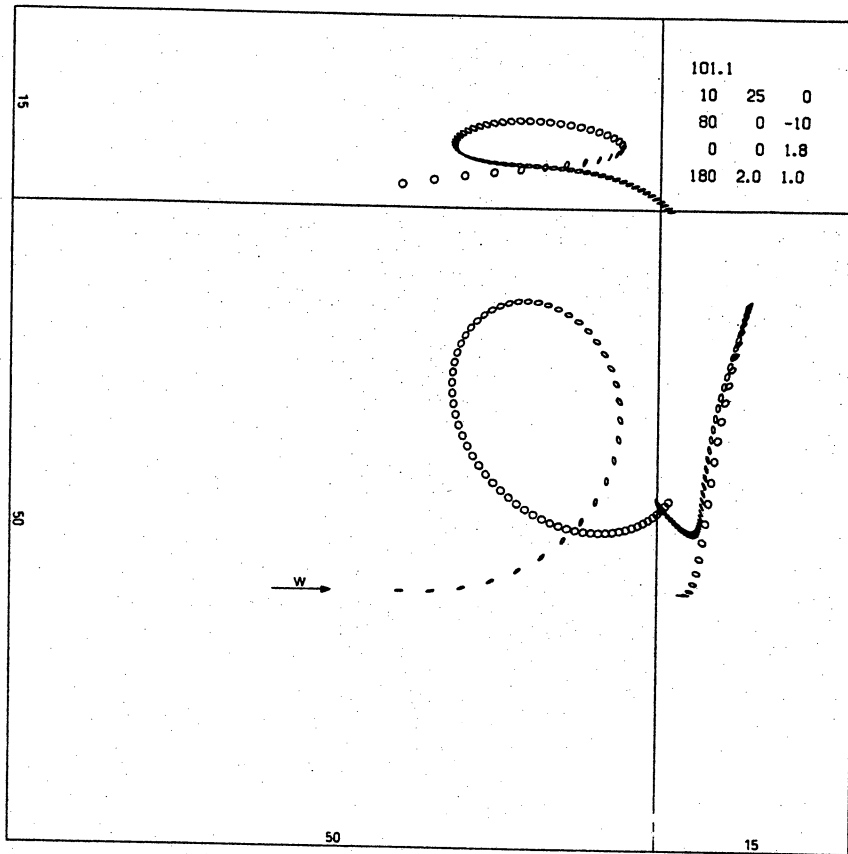


fig. 29.3e

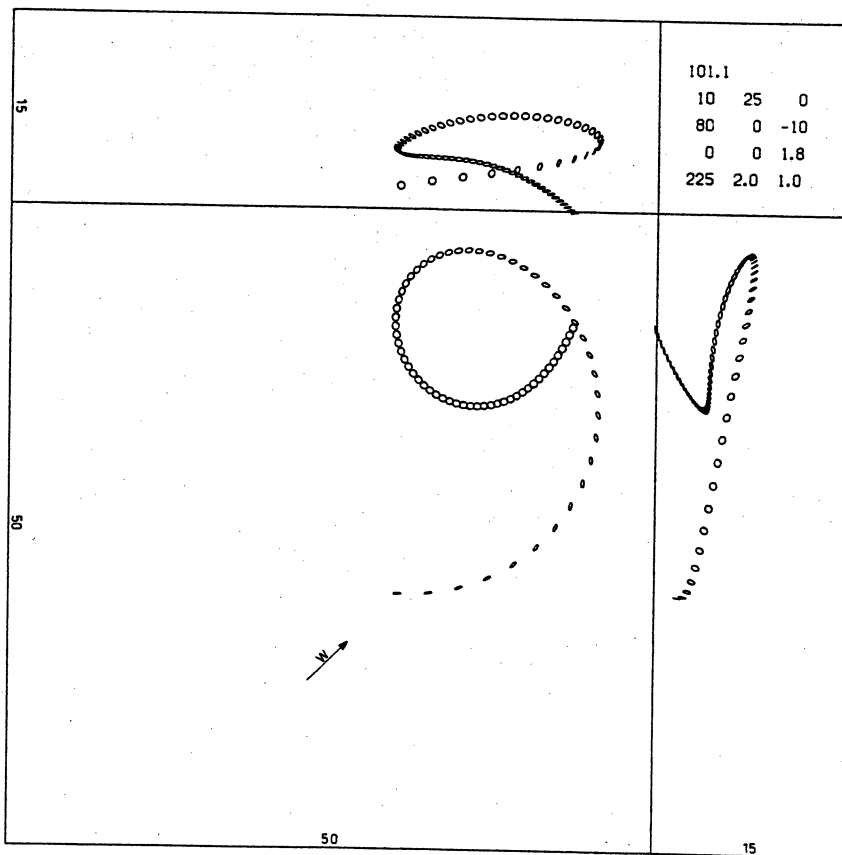


fig. 29.3f

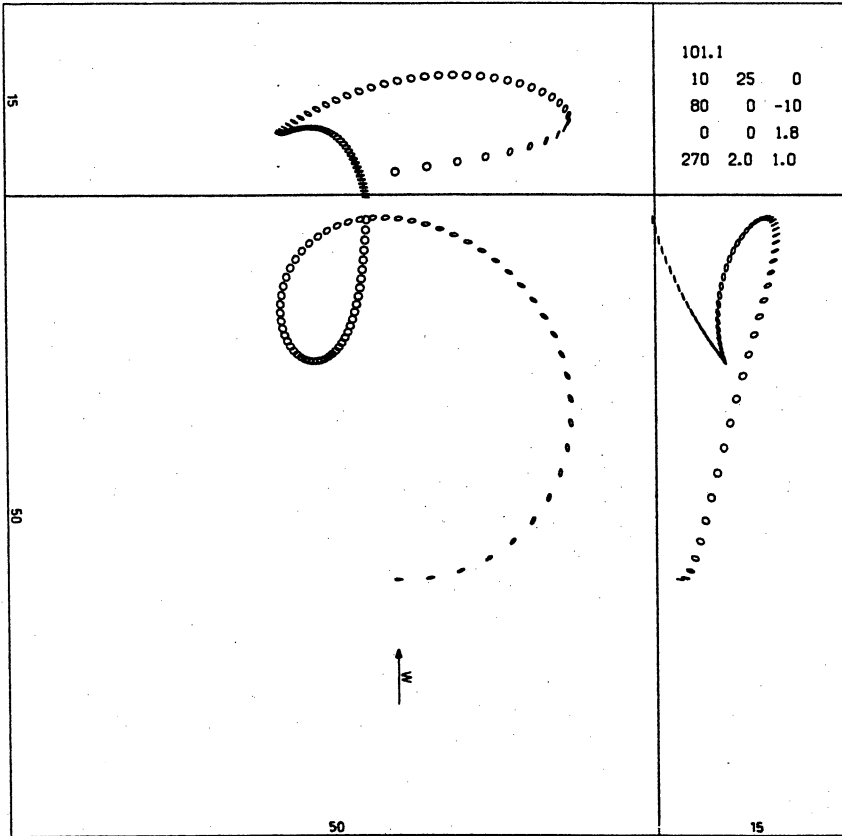


fig. 29.3g

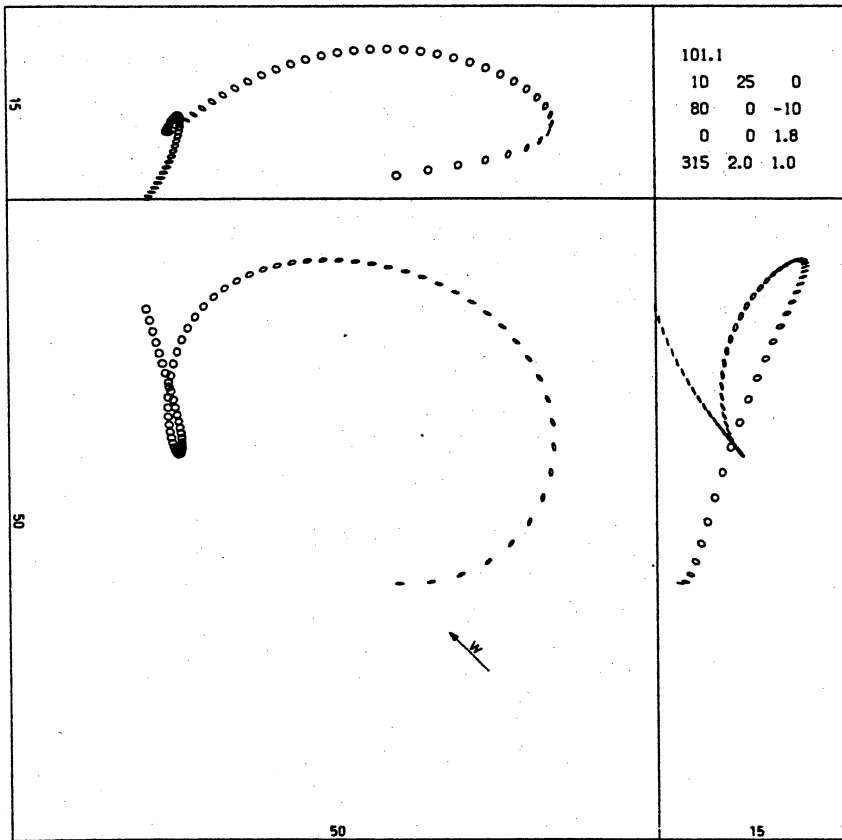


fig. 29.3h

§30 Mass distribution:  $m$  and  $I_3$ .

Two experimental examples showing the influence of a change in a boomerang's mass distribution on the diameter of the flight path are given in fig. 30.1 and fig. 30.2. These contain level 1 flight path stereograms for boomerang L1 plain and boomerang L1 weighted.

	a (m)	m (kg)	$I_3$ (kg. m <sup>2</sup> )	$\lambda$
L1 plain	.298	.173	.00396	.258
L1 weighted	.298	.188	.00455	.272
difference	0	9%	15%	5.5%

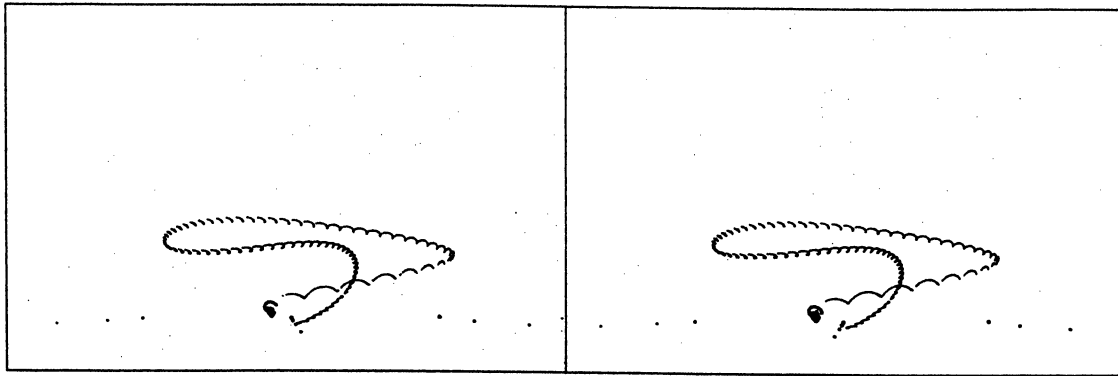
Table 30.1. Mass distribution for L1 plain and L1 weighted.  $\lambda = I_3/ma^2$ .

The stereograms of fig. 30.1 are roughly similar in shape, they indicate a flight path diameter of about 22 m for the L1 plain, and about 28 m for the L1 weighted.

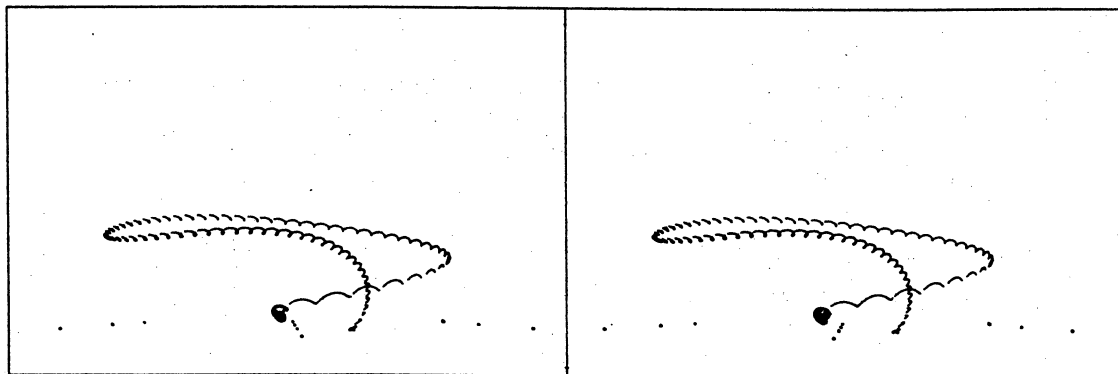
To investigate the influence of  $m$  and  $I_3$  on boomerang flights, a number of model boomerangs were used, based on boomerang 101.1 (level 2), but with different values for  $m$  and  $I_3$ . They are listed in tabel 30.2. Boomerang 101.6 is almost identical with boomerang 101.1, the other six boomerangs differ by a factor 2 either in  $m$  or in  $I_3$  or in both.

boomerang nr.	m (kg)	$I_3$ (kg. m <sup>2</sup> )	$\lambda$
101.3	.080	.0020	.282
101.4	.160	.0020	.141
101.5	.080	.0040	.564
101.6	.160	.0040	.282
101.7	.320	.0040	.141
101.8	.160	.0080	.564
101.9	.320	.0080	.282

Table 30.2. Mass distributions for the 7 model boomerangs.

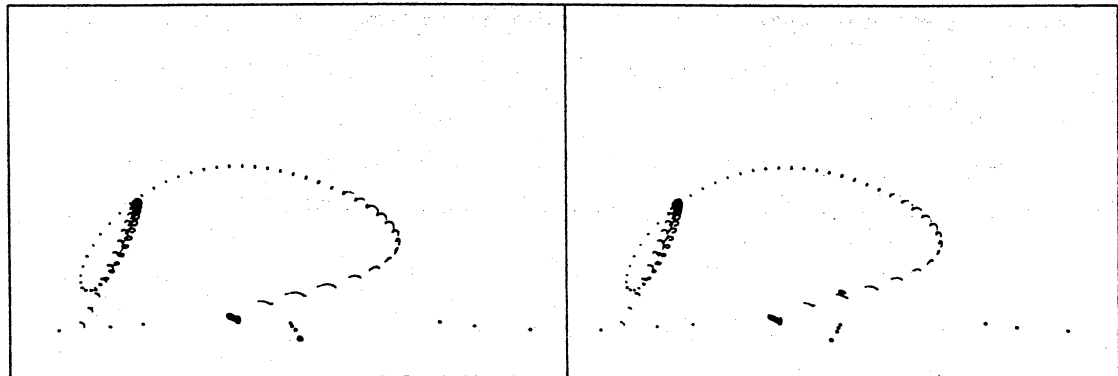


a

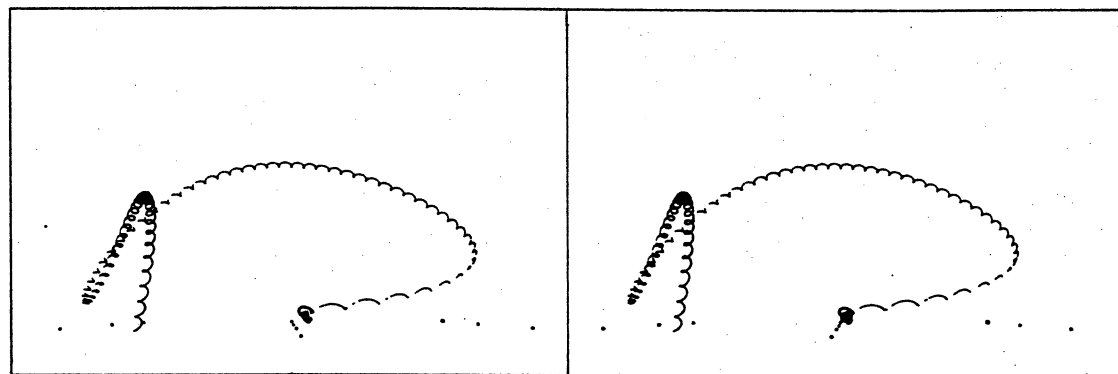


b

fig. 30.1. a: L1 plain, {1}, 7R6/L6A. b: L1 weighted, {1}, 11R19A/L19.



a



b

fig. 30.2. a: L1 plain, {1}, 4R8/L7A. b: L1 weighted, {2}, 11R9A/11L9.

Figure 30.1a through h shows 8 flight paths computed for these boomerangs. In 7 of these the initial conditions are:

$f_0 = 10 \text{ rev/s}$ ,  $V_0 = 25 \text{ m/s}$ ,  $\Psi_0 = 0^\circ$ ,  
 $\theta_0 = 80^\circ$ ,  $\phi_0 = 0^\circ$ ,  $\psi_0 = -10^\circ$ ,  
 $X_0 = 0 \text{ m}$ ,  $Y_0 = 0 \text{ m}$ ,  $Z_0 = 1.8 \text{ m}$ ,  
 no wind.

The additional flight for boomerang 101.9 has the same initial conditions, except that  $f_0 = 12 \text{ rev/s}$ ,  $V_0 = 30 \text{ m/s}$ .

bnr	t	P	n	D	Z <sub>2</sub>	D <sub>2</sub>	D <sub>1</sub>	f <sub>2</sub>	f <sub>1</sub>	V <sub>1</sub>	Ψ <sub>2</sub>	U <sub>1</sub>
101.3	8.4	66.9	56.4	3.6	9.6	11.6	1.3	10.0	5.9	2.1	24.2	.19
101.4	2.8	32.4	29.5	9.0	7.8	10.2	9.1	12.7	8.7	7.3	25.2	.34
101.5	7.7	85.1	49.8	21.9	3.5	33.5	19.0	10.0	5.5	4.0	20.2	.38
101.6	8.3	81.6	72.6	11.6	9.8	23.4	2.4	10.0	8.2	3.2	33.8	.20
101.7	3.2	41.1	37.6	17.6	7.1	21.5	17.6	12.7	9.9	7.4	28.1	.31
101.8	1.7	37.1	15.6	34.7	3.1	34.7	-	10.0	8.5	20.3	0.6	1.25
101.9	5.7	84.7	59.1	30.7	5.8	43.4	30.7	10.9	9.6	8.7	16.9	.43
101.9	9.2	125.9	106.9	12.0	11.5	45.6	10.4	12.2	11.3	4.2	45.0	.18

Table 30.3. Some values for the flights of fig. 30.1. Last row:  $f_0 = 12$ ,  $V_0 = 30$ . Flight of 101.5 has minimum  $\Psi = -1.2^\circ$ . Flight of 101.8 has minimum  $\Psi = -0.7^\circ$ , D is increasing as the 101.8 reaches  $Z = 0$ .

Some values for the 8 flights of fig. 30.1 are listed in table 30.3. The relatively large differences in m and/or  $I_3$  obviously give rise to dramatic differences in the shape of the flight paths. Boomerangs with equal values for  $\lambda$  have more or less similarly shaped flight paths which differ primarily in size. This rough similarity can also be observed in table 30.4, which lists some values of the flights at the instant at which  $\dot{\Psi} = 0$  occurs for the first time. It is evident that boomerangs with low  $\lambda$  reach high values of  $\Psi$  and reversely. Again this phenomenon can be explained on the basis of the exposition given in the second half of §22.

In §7 it was shown that boomerangs such as 101.3, 101.6 and 101.9, which differ only in average density, but have the same  $\lambda$ , can traverse exactly similar flight paths, provided they are launched at the appropriate

bnr	t	f	V	U	$\Psi$
101.3	0.3	9.5	21.2	1.20	6.9
101.4	0.5	11.9	14.6	0.65	24.2
101.5	0.6	8.8	20.1	1.22	-1.2
101.6	0.8	9.5	19.4	1.09	7.8
101.7	1.0	11.9	13.6	0.61	28.1
101.8	0.5	9.5	22.6	1.27	-0.7
101.9	not reached				

Table 30.4. First instant  $t$  at which  $\dot{\Psi} = 0$  occurs, and values of  $f, V, U, \Psi$  at that instant.

speed and spin. Suppose that, in accordance with table 7.1, row 3, we launch the three boomerangs with values for  $f_0$  and  $V_0$  as listed in table 30.5. Then we know that the flight path diameter for boomerang 101.3 is half that for boomerang 101.6, and that the flight path diameter of boomerang 101.9 is twice that for boomerang 101.6. The corresponding values for  $D_2$  are listed in table 30.5. It is interesting to note that these values do not deviate much from those listed in table 30.3. This again shows that the flight path diameter is not very sensitive to the speed at which a boomerang is launched (provided that  $U_0$  is constant, see §26).

bnr	$f_0$	$V_0$	$D_2$
101.3	7.1	17.7	11.7
101.6	10.0	25.0	23.4
101.9	14.1	35.4	46.8

Table 30.5. Some values for similar flight paths.

It may be interesting to note the influence of the insertion of batteries in the elbow of an experimental boomerang. This increases  $m$ , but hardly  $I_3$  (see §10). The addition of the batteries' mass causes the boomerang's angle of incidence to increase, which decreases the resulting flight path diameter. To a somewhat exaggerated degree this effect can be seen by comparing the computed flights for boomerangs 101.3 and 101.4 in fig. 30.3a and b, or the flights for boomerangs 101.5, 101.6 and 101.7 in fig. 30.3c,d and e.

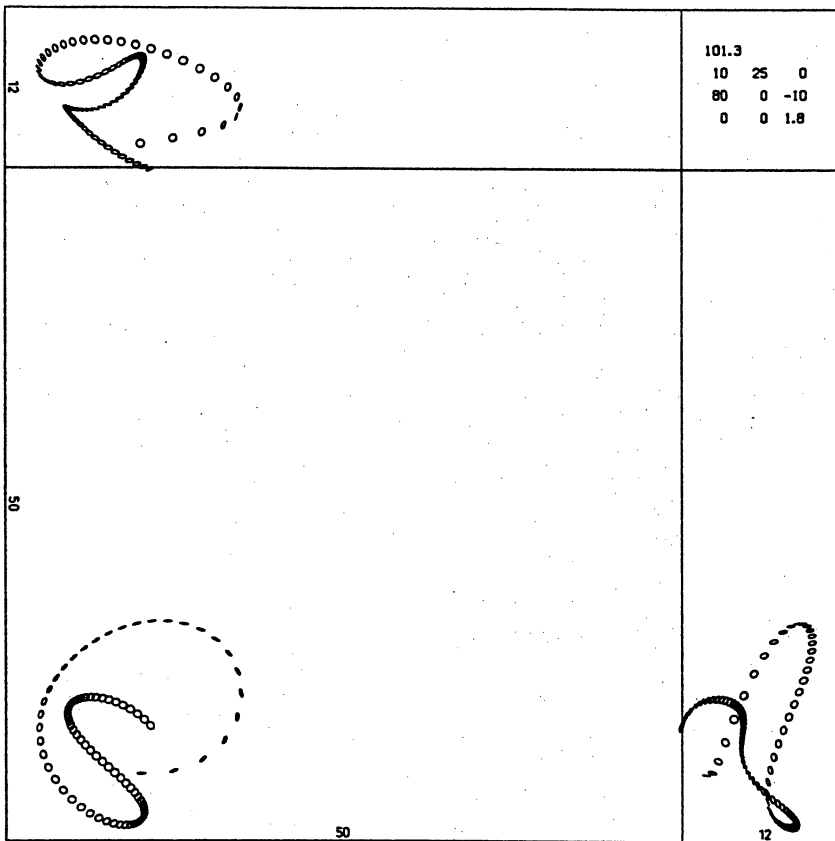


fig. 30.3a

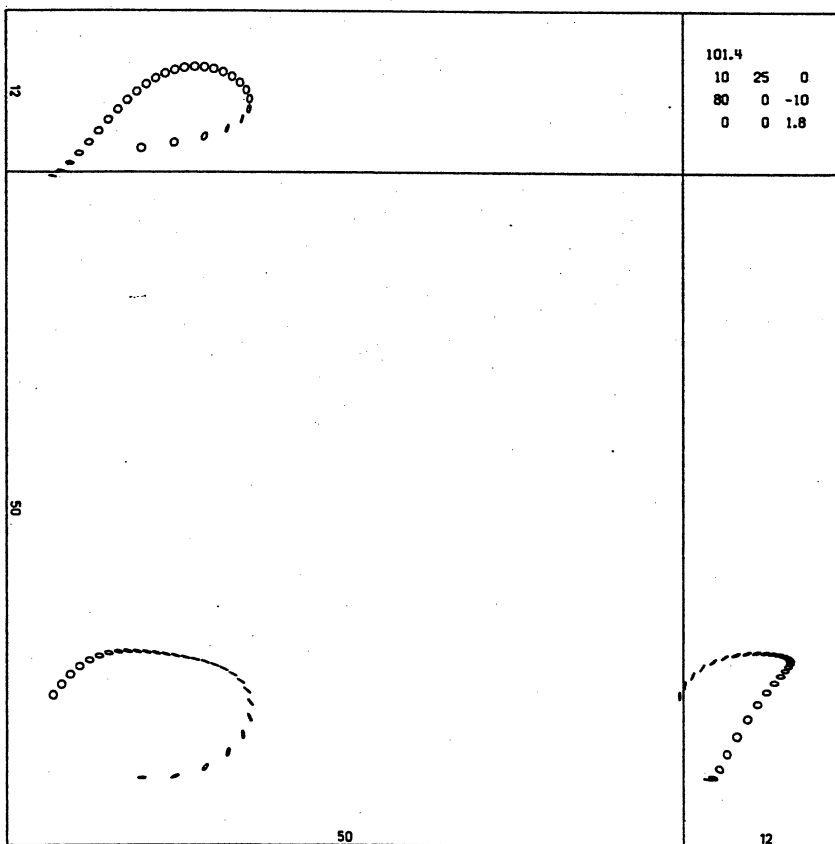


fig. 30.3b

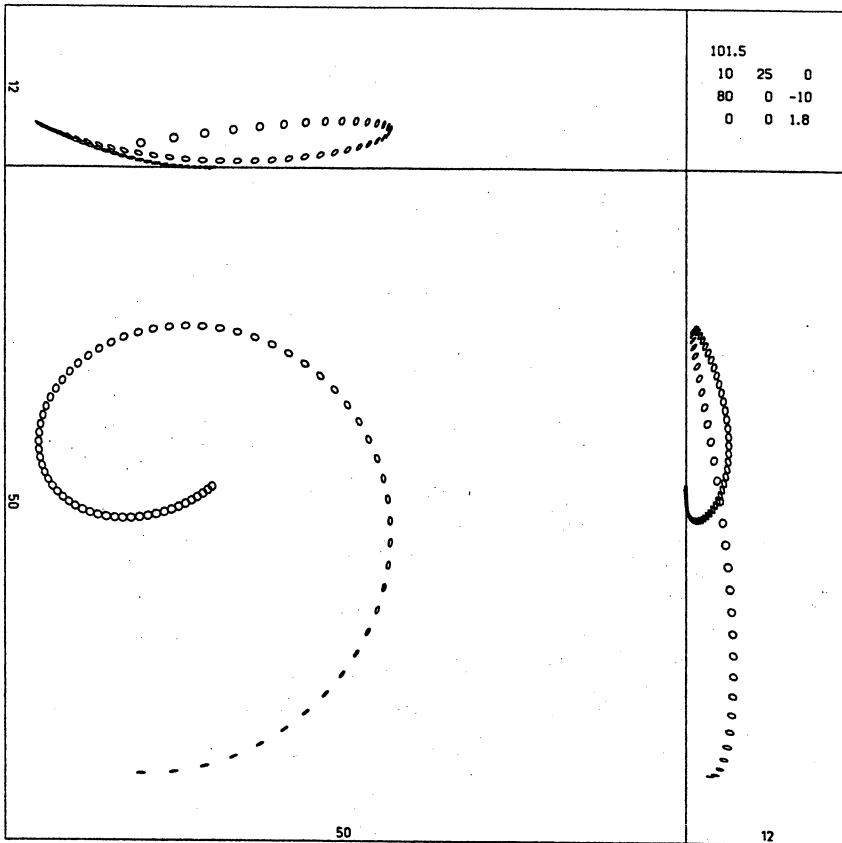


fig. 30.3c

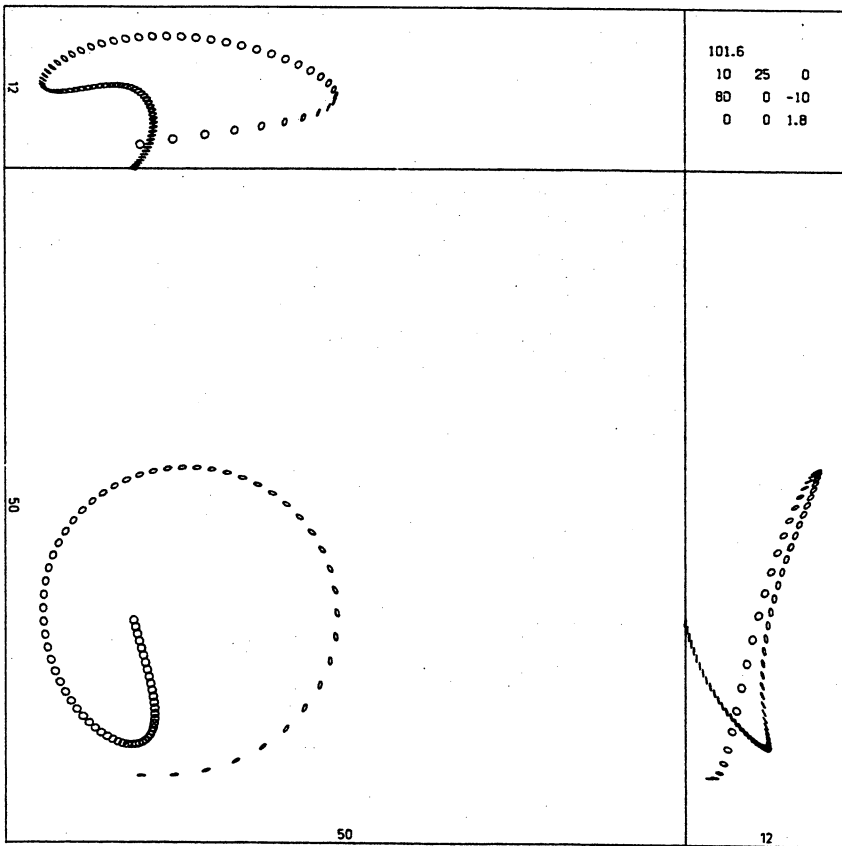


fig. 30.3d

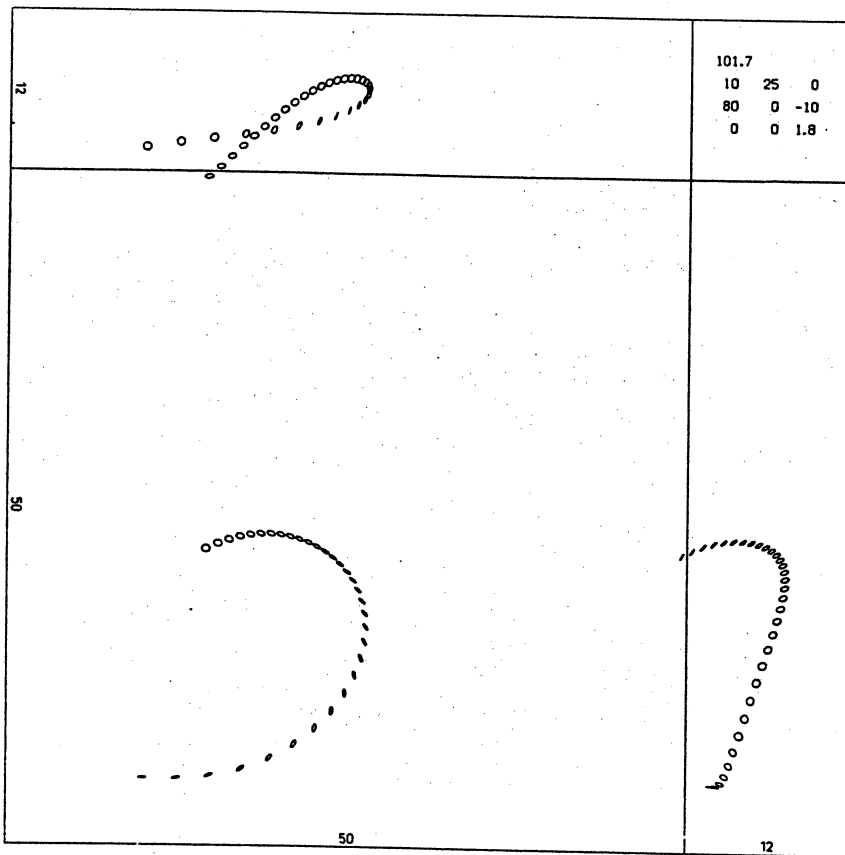


fig. 30.3e

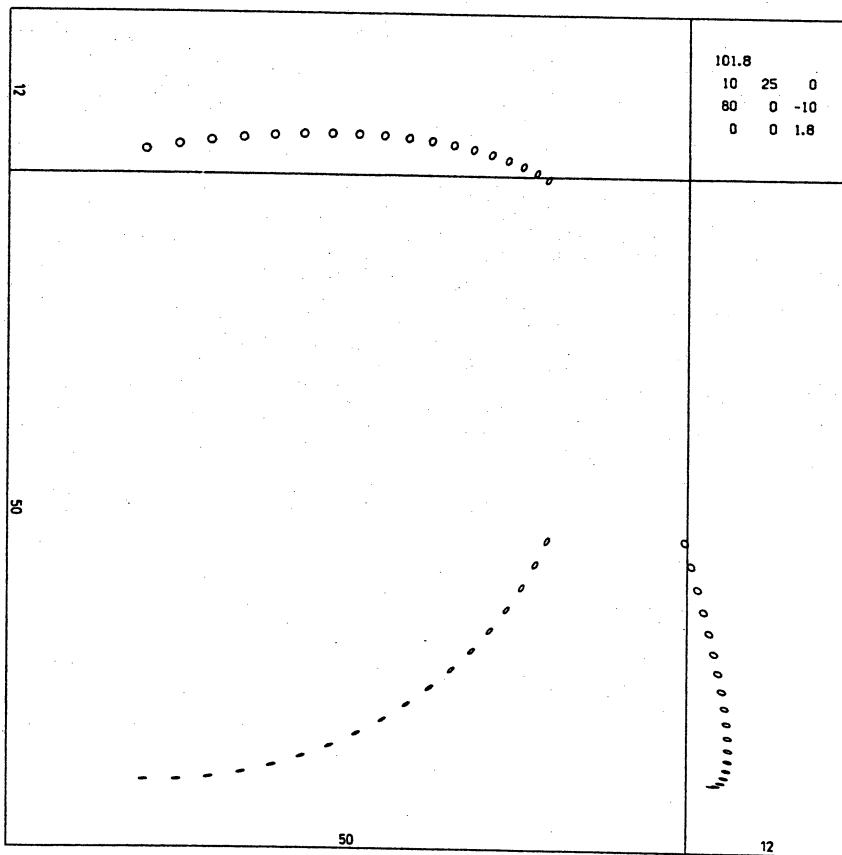


fig. 30.3f

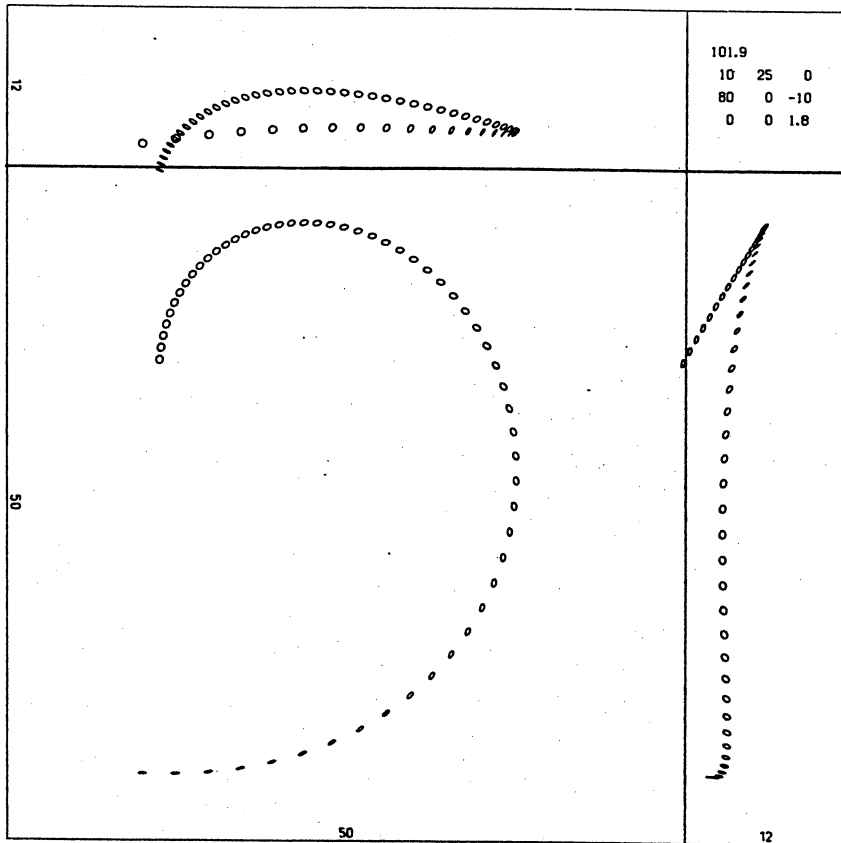


fig. 30.3g

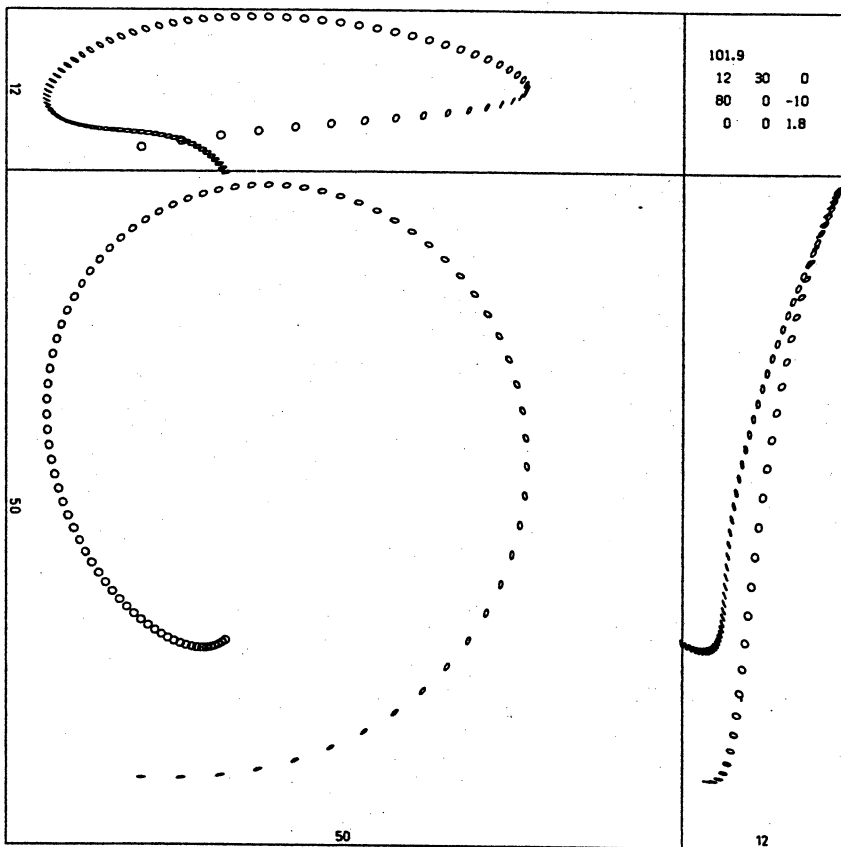


fig. 30.3h

§31 Maximum lift coefficient  $C_{L2}$ .

$C_{L2}$  is the maximum lift coefficient for a boomerang arm's profile. In Part II, §22 the parameters characterizing the aerodynamic properties of level 3 model boomerangs are defined (see especially Part II, fig. 22.1). For moderate angles of incidence  $\alpha^*$  ( $\alpha_1 \leq \alpha^* \leq \alpha_2$ ) the profile lift coefficient  $C_L$  varies linearly with  $\alpha^*$ . At  $\alpha^* = \alpha_2$   $C_L$  reaches its maximum value  $C_{L2}$ . For higher values of  $\alpha^*$  stall occurs, and  $C_L$  decreases below  $C_{L2}$ .

The wind tunnel experiments reported in Part II, §26 indicated a value for  $C_{L2}$  of about 1.2 at most. The measurements were done on boomerang arms put in a straight airflow. In Part II, §32 it was shown that such low values of  $C_{L2}$  are unrealistic for boomerang arms forming part of *rotating* boomerangs. One of the reasons for including the present section is that it shows how poor the flight performance is of model boomerangs having arms with  $C_{L2} = 1.2$ .

boomerang nr.	normal profile $C_{L2}$	reversed profile $C_{L2}$
222.1	1.2	1.2
217.1	1.6	2.4
195.1	2.0	2.4
260.1	4.0	4.0

Table 31.1.  $C_{L2}$  values of model boomerangs.

Figure 31.1a through d shows 4 flight paths traversed by boomerangs differing only in  $C_{L2}$  and being otherwise identical with level 3 boomerang 195.1 (which is associated with boomerang L1 plain), see Part II, table 32.1. Table 31.1 lists the  $C_{L2}$  values for these boomerangs. The initial conditions in all 4 cases are:

$$f_o = 11 \text{ rev/s}, V_o = 27 \text{ m/s}, \psi_o = 0^\circ,$$

$$\theta_o = 90^\circ, \phi_o = 0^\circ, \psi_o = -20^\circ,$$

$$X_o = 0 \text{ m}, Y_o = 0 \text{ m}, Z_o = 1.8 \text{ m},$$

no wind.

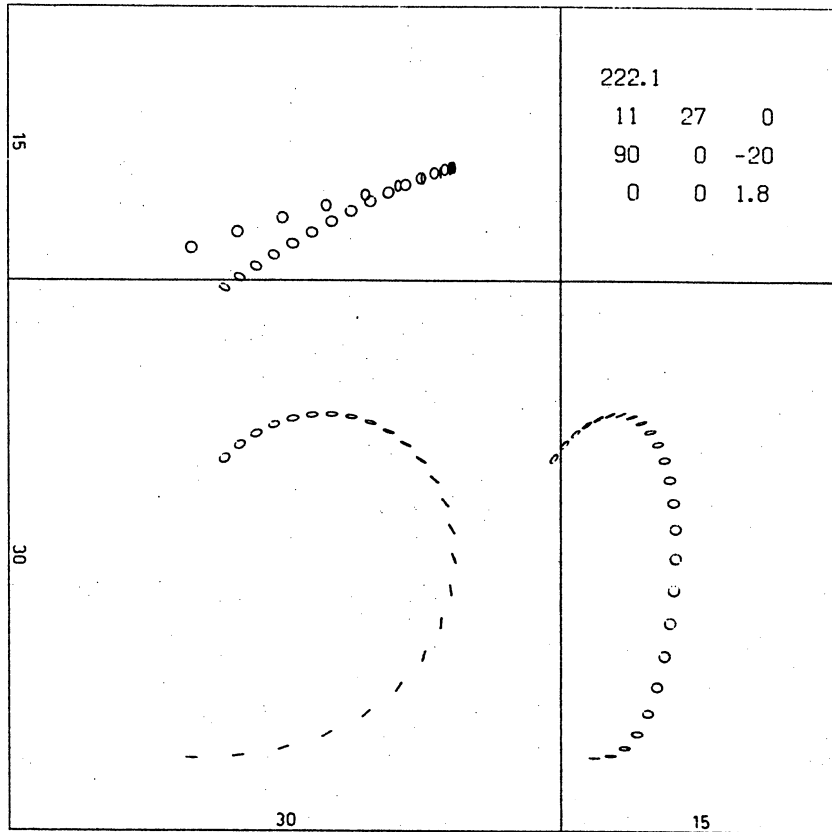


fig. 31.1a

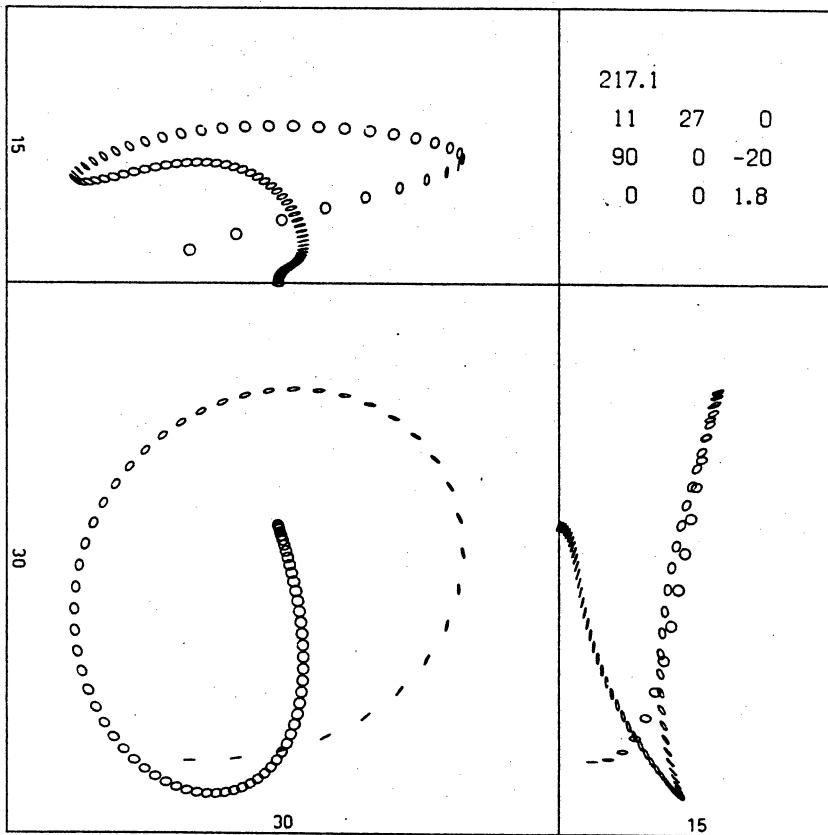


fig. 31.1b

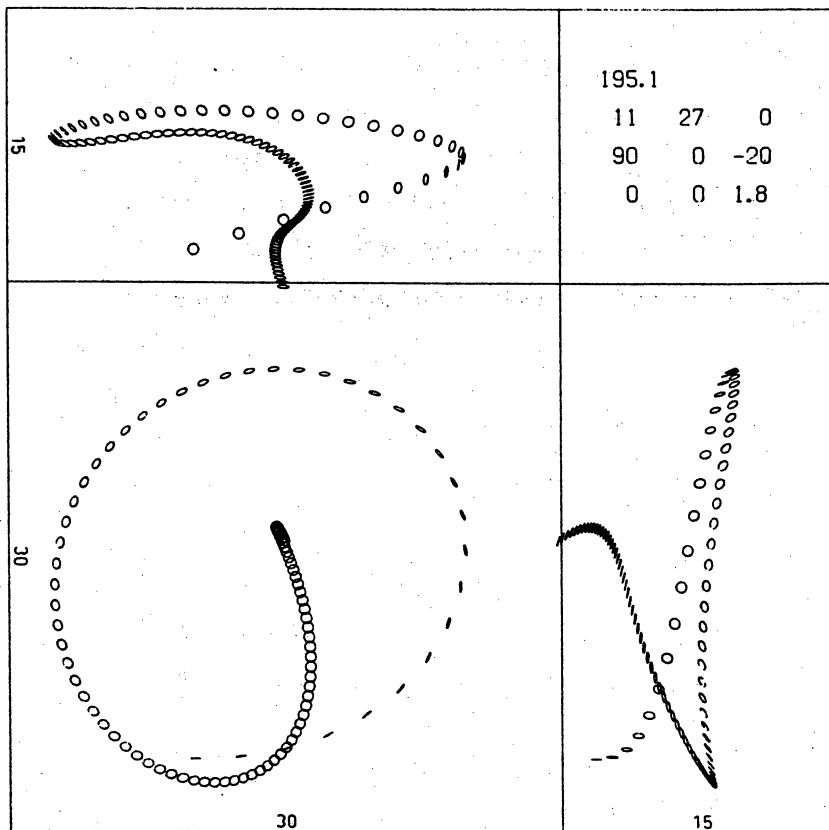


fig. 31.1c

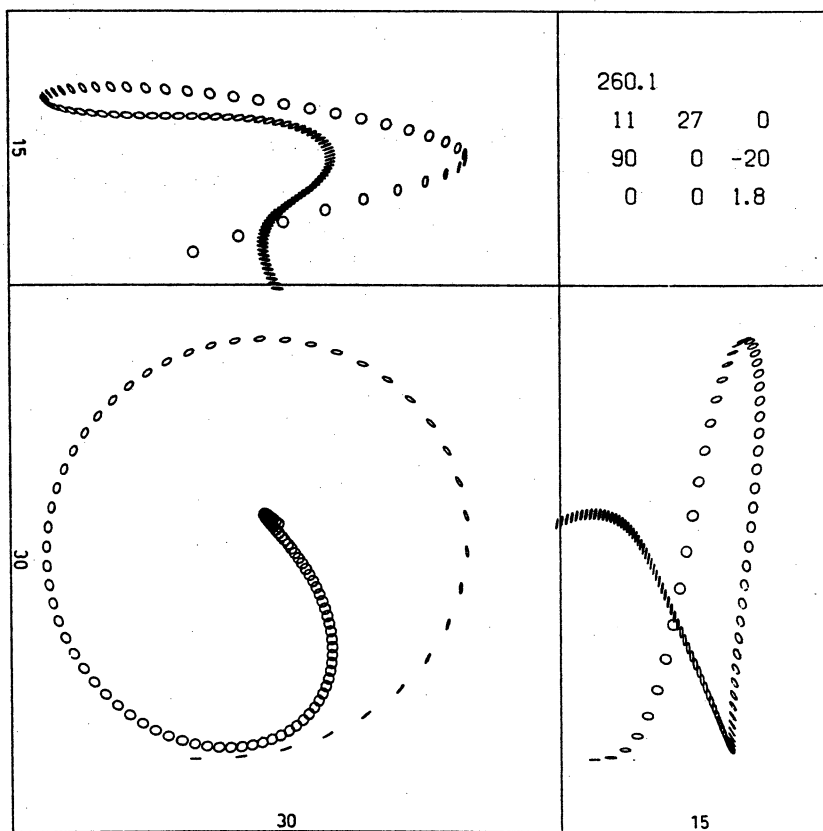


fig. 31.1d

Fig. 31.1a clearly indicates that boomerang 222.1 is a very poor boomerang indeed. The three other boomerangs all perform satisfactory return flights. In tables 31.2 and 31.3 some values for the flights are listed. The 4 flight paths differ significantly in maximum elevation ( $Z_2$ ), which increases with increasing  $C_{L2}$ . Table 31.3 gives values of  $f, V, U$  and  $\psi$  at  $t = 1.1$  sec. (Approximately at this instant  $\dot{\psi} = 0$  occurs for the first time in each of the flights.) We see: the lower  $C_{L2}$ , the stronger the initial decrease of  $V$ , and the higher the resulting value of  $\psi$ .

bnr	t	P	n	D	$Z_2$	$D_2$	$D_1$	$f_2$	$f_1$	$V_1$	$\psi_2$	$U_1$
222.1	2.4	39.8	24.5	16.4	6.2	20.7	16.4	11.0	9.9	11.9	21.3	.64
217.1	8.7	87.4	84.8	13.7	8.2	21.7	1.6	11.0	9.3	1.5	88.0	.08
195.1	10.2	92.3	99.1	12.9	9.4	22.3	1.2	11.0	9.4	1.7	85.7	.09
260.1	11.0	96.5	104.5	13.7	10.8	23.7	0.8	11.0	8.5	2.2	83.7	.13

Table 31.2. Some values for the flights of fig. 31.1.

bnr	t sec	f rev/s	V m/s	U	$\psi$ degr
all	0	11.0	27.0	1.31	0.0
222.1	1.1	10.2	14.4	0.76	20.9
217.1	1.1	10.3	17.8	0.92	12.9
195.1	1.1	10.3	18.3	0.93	10.9
260.1	1.1	10.2	19.0	1.00	8.7

Table 31.3. Some values for the flights after 1.1 sec.

§32 *The width of boomerang arms.*

According to Part II, §22, the width of a model boomerang arm is determined by giving the chord length  $c_t$  at the tip and  $c_r$  at the root of the arm. In this section we consider three boomerangs having arms with constant chord, i.e. with  $c_t = c_r$ . These boomerangs differ from each other in chord, but their other aerodynamic parameters are identical with those of level 3 boomerang 239.1 (which is associated with boomerang WU), see Part II, table 32.1. Values for the chord lengths and for the mass distributions of the boomerangs to be compared are listed in table 32.1

boomerang nr	chord arm 1 (m)	chord arm 2 (m)	m (kg)	$I_3$ (kg.m <sup>2</sup> )
244.2	.020	.020	.080	.0228
239.1	.040	.039	.160	.0456
267.3	.060	.060	.240	.0684

Table 32.1. Parameters in which the 3 boomerangs differ ( $a = .296$  m).

The chords of the three boomerangs are in the proportion 1:2:3 (with a slight deviation for arm nr. 2 of boomerang 239.1). The values for  $m$  and  $I_3$  are based on those for boomerang 239.1 and are chosen in the same proportion 1:2:3. Why are  $m$  and  $I_3$  chosen this way? The differences in chord lead to corresponding differences in the aerodynamic forces. These in turn would lead to predictable differences in the flight paths if  $m$  and  $I_3$  would be constant: the boomerang with the broadest arms would have the smallest flight path diameter. On the other hand, if the three boomerangs would have similar profiles, and be made of the same material, the masses would be in the proportion 1:4:9. The influence of mass would now be predominant, and the boomerang with the broadest arms would have the largest flight path diameter.

In the following discussion we refer to the winglet model described in Part II, §2. If the chords of the boomerang arms are multiplied by a constant factor  $f$ , the winglets' density in the circular region

S is multiplied by  $f$  also. As long as the winglets' density is very small, the lift distribution on the winglet system (at given  $V$ ,  $\omega_z$ ,  $\psi$ ) changes by the same factor  $f$ . At higher densities, however, the lift distribution does not change proportionally, but, for instance, the peak at the leading edge of S grows relatively stronger. (The theoretical background is discussed in Part II, §4.) This leads us to expect that the ratio  $T_{1y}/F_{1z}$  increases with increasing chord lengths. This is indeed confirmed by table 32.2, which lists some data taken from numerical computations for the aerodynamic forces on the three model boomerangs.  $T_{1x}/F_{1z}$ ,  $T_{1y}/F_{1z}$ ,  $T_{1y}/T_{1x}$  all appear to be increasing with increasing chord, while  $F_{1z}$  increases less than proportionally with chord length

bnr	$\frac{2c}{2\pi a}$	$F_{1z}$	$\frac{T_{1x}}{F_{1z}}$	$\frac{T_{1y}}{F_{1z}}$	$\frac{T_{1y}}{T_{1x}}$
244	.00215	.0474	.249	.036	.145
239	.00425	.0809	.264	.057	.219
267	.00645	.1094	.267	.079	.295

Table 32.2. Some aerodynamic data at  $\psi = 5^\circ$ ,  $U = 1$ .  
c = chord.

In the present section we wish to show the influence of this change in the shape of the lift distribution (due to a change in chord) on a boomerang's flight. Therefore the boomerangs'  $m$  and  $I_3$  are chosen in such a way, that *if* the lift distributions were similarly shaped and have magnitudes in the proportion 1:2:3, the resulting flight paths would be identical. In this hypothetical case, the aerodynamic forces, the gravitational forces and the inertial forces all would be in the proportion 1:2:3, provided the boomerangs would be similarly launched.

The flights computed for the three boomerangs have the initial conditions:

$f_o = 10$  rev/s,  $V_o = 25$  m/s,  $\psi_o = 0^\circ$ ,  
 $\theta_o = 70^\circ$ ,  $\phi_o = 0^\circ$ ,  $\psi_o = -10^\circ$ ,  
 $X_o = 0$  m,  $Y_o = 0$  m,  $Z_o = 1.8$  m,  
 no wind.

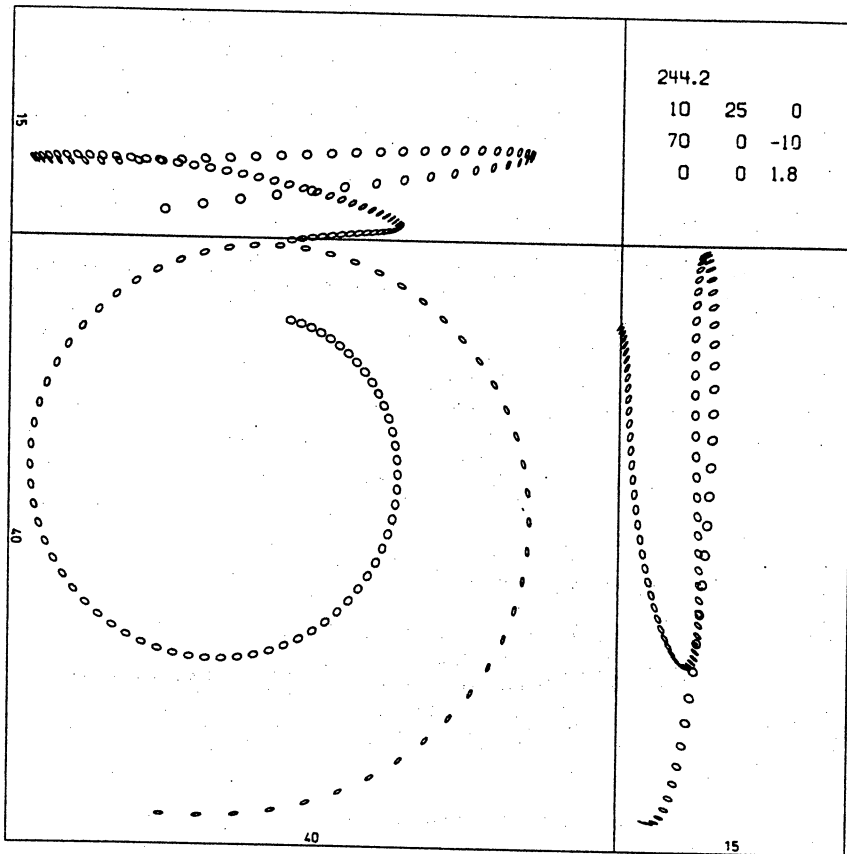


fig. 32.1a

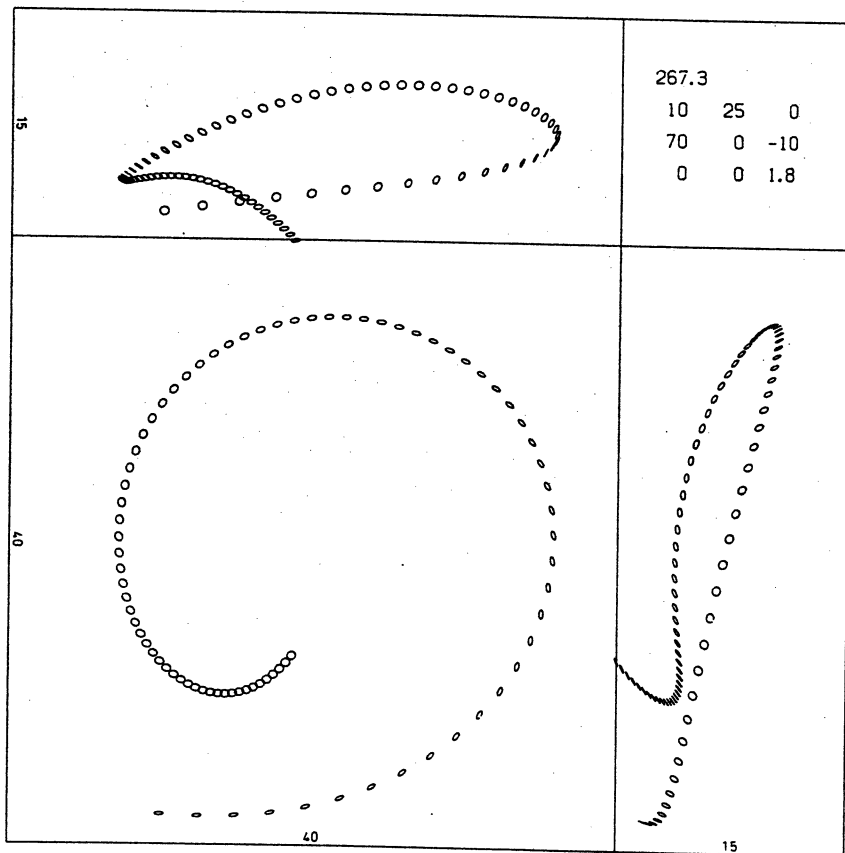


fig. 32.1b

Figure 32.1 shows that the flight paths of the boomerangs 244.2 and 267.3 differ appreciably. The corresponding flight path of boomerang 239.1 is shown in fig. 21.1 b. Some values for the three flights are listed in table 32.3.

bnr	t	P	n	D	$Z_2$	$D_2$	$D_1$	$f_2$	$f_1$	$V_1$	$\Psi_2$	$U_1$
244.2	9.8	139.0	86.1	33.7	6.0	38.6	10.6	10.0	8.3	7.1	12.9	.41
239.1	8.5	115.1	78.6	22.7	8.2	36.6	9.6	10.0	8.9	8.0	15.2	.45
267.3	8.2	102.8	76.2	13.6	10.3	36.2	8.7	10.0	8.9	5.2	22.0	.29

Table 32.3. Some values of the flights discussed in this section.

The most obvious difference between the three flight paths concerns the maximum elevation ( $Z_2$ ). Boomerang 244.2 remains very low throughout its flight, but boomerang 267.3 comes considerably higher. This difference can be traced to the differences in the lift distributions mentioned above. The relatively large increase of the pitching torque  $T_y$  with increasing chord causes the boomerang with the greatest chord to lie down fastest. Indeed, after flying for one second, the angle  $\theta$  has changed from its initial value  $\theta_0 = 70^\circ$ , to  $70.2^\circ$  for boomerang 244.2, to  $66.9^\circ$  for boomerang 239.1, and to  $62.9^\circ$  for boomerang 267.3.

§33 *Twist.*

Both this section and the following one deal with changes in the parameter  $\alpha_{ot}$ , which is the geometrical angle of incidence relative to the direction of zero lift, for the profile near the tip of a boomerang arm (see Part II, §22). If a boomerang arm is given a positive twist, its  $\alpha_{ot}$  is increased (and the  $\alpha_{ot}$  for the reversed profile is decreased, of course). In this section we compare boomerangs having both arms either positively or negatively twisted relative to level 3 boomerang 195.1. Otherwise the boomerangs are the same (see Part II, table 32.1). Table 33.1 lists the respective values of  $\alpha_{ot}$  for the three boomerangs considered.

boomerang nr.	arm nr. 1		arm nr. 2	
	normal	reversed	normal	reversed
264.1	+2.0°	+2.0°	-1.0°	+5.0°
195.1	+5.0°	-1.0°	+2.0°	+2.0°
261.1	+8.0°	-4.0°	+5.0°	-1.0°

Table 33.1.  $\alpha_{ot}$  for the model boomerangs.

If one would twist both arms of boomerang 195.1 so that the tips would become inclined 3° more upward, one would obtain boomerang 261.1, and if one would apply a negative twist of equal magnitude to the arms of boomerang 195.1, one would obtain boomerang 264.1. It is obvious that for given  $V$ ,  $\omega_z$  and  $\Psi \geq 0$ , boomerang 261.1 experiences more lift, especially near the tips, than boomerang 264.1 does. Some data relevant to the effect of twist on the aerodynamic forces (at  $\Psi = 10^\circ$ ,  $U = 1$ ) are listed in table 33.2. We see that  $F_{1z}$ ,  $T_{1x}$  and  $T_{1y}$  all increase with increasing twist, but  $T_{1y}$  increases very little. In particular, the ratio  $T_{1y}/T_{1x}$  decreases with increasing twist.

bnr	$F_{1z}$	$T_{1x}$	$T_{1y}$	$\frac{T_{1x}}{F_{1z}}$	$\frac{T_{1y}}{F_{1z}}$	$\frac{T_{1y}}{T_{1x}}$
264.1	.1478	.0315	.0125	.213	.085	.398
195.1	.1644	.0401	.0131	.244	.080	.327
261.1	.1808	.0488	.0138	.270	.076	.282

Table 33.2. Some aerodynamic values at  $\Psi = 10^\circ$ ,  $U = 1$ .

Let us now consider the flight paths of these boomerangs, shown in fig. 33.1a, b, c. They are computed with the initial conditions:

$$f_0 = 11 \text{ rev/s}, V_0 = 27 \text{ m/s}, \psi_0 = 0^\circ,$$

$$\theta_0 = 90^\circ, \phi_0 = 0^\circ, \psi_0 = -20^\circ,$$

$$X_0 = 0 \text{ m}, Y_0 = 0 \text{ m}, Z_0 = 1.8 \text{ m},$$

no wind.

Some values for these flights are listed in table 33.3.

bnr	t	P	n	D	Z <sub>2</sub>	D <sub>2</sub>	D <sub>1</sub>	f <sub>2</sub>	f <sub>1</sub>	V <sub>1</sub>	ψ <sub>2</sub>	U <sub>1</sub>
264.1	8.4	103.0	74.5	18.6	16.2	44.0	18.5	11.0	7.9	2.0	38.6	.11
195.1	10.2	92.3	99.1	12.9	9.4	22.3	1.2	11.0	9.4	1.7	85.7	.09
261.1	5.5	60.8	52.6	2.2	6.1	15.0	1.8	11.0	8.5	4.2	18.6	.25

Table 33.3. Some values for the flights of fig. 33.1.

The three flight paths have widely different sizes ( $Z_2, D_2$ ). Obviously, a twist of  $3^\circ$  can dramatically alter a boomerang's flight path. Table 33.4 lists some values at  $t = 1$  sec. At this instant the angle  $\psi$  is highest for boomerang 261.1 and lowest for boomerang 264.1, which is in accordance with the difference in flight path curvature for these boomerangs. From fig. 33.1 boomerang 264.1 appears to lie down faster than boomerang 261.1. This is confirmed by table 33.4: after 1 sec,  $\theta$  has varied relatively fast, and  $\phi$  relatively slowly for boomerang 264.1.

bnr	t sec	f rev/s	V m/s	U	ψ degr	θ degr	φ degr	ψ degr
all	0	11.0	27.0	1.31	0.0	90.0	0.0	-20.0
264.1	1.0	9.0	22.6	1.35	1.8	71.8	39.2	- 3.8
195.1	1.0	10.3	19.1	0.99	10.8	77.5	113.1	-12.8
261.1	1.0	10.6	13.7	0.69	13.4	84.2	155.8	- 1.1

Table 33.4. Some values for the flights at  $t = 1$  sec.

The data presented in this section indicate that even a slight amount of twist in a boomerang's arms may have a significant effect on the flight path.

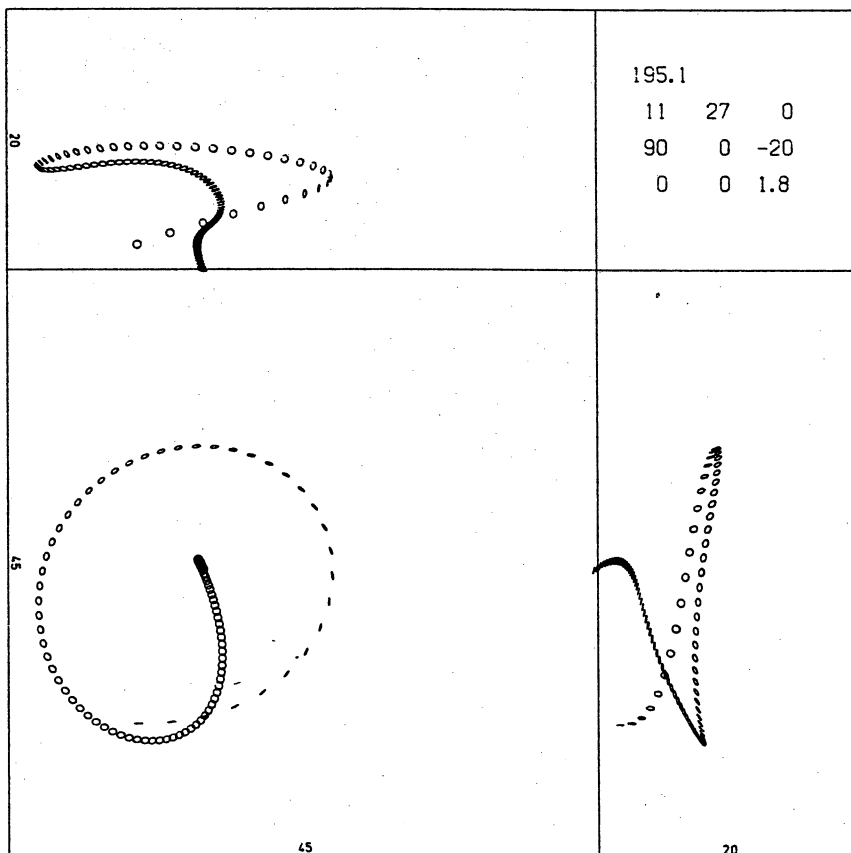


fig. 33.1a

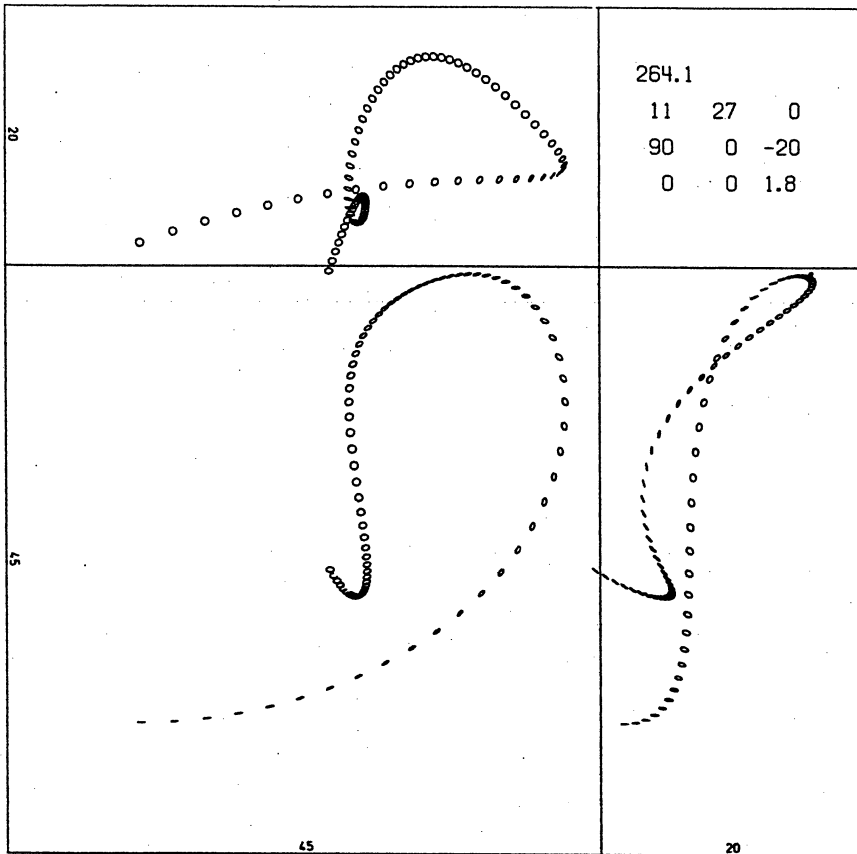


fig. 33.1b

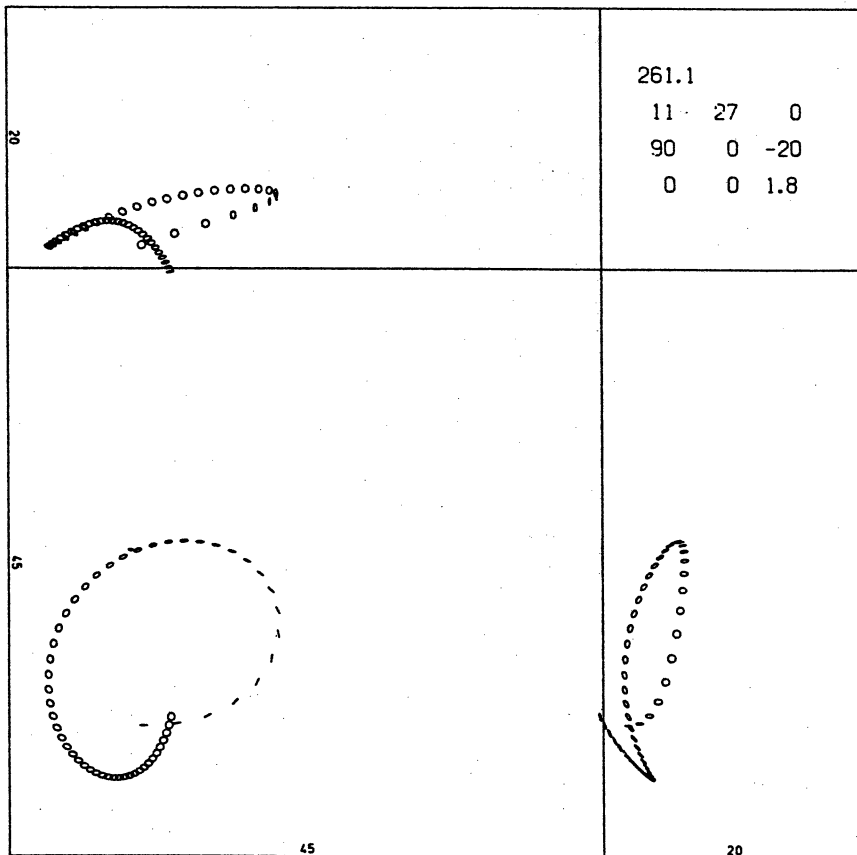


fig. 33.1c

§34 Dihedral.

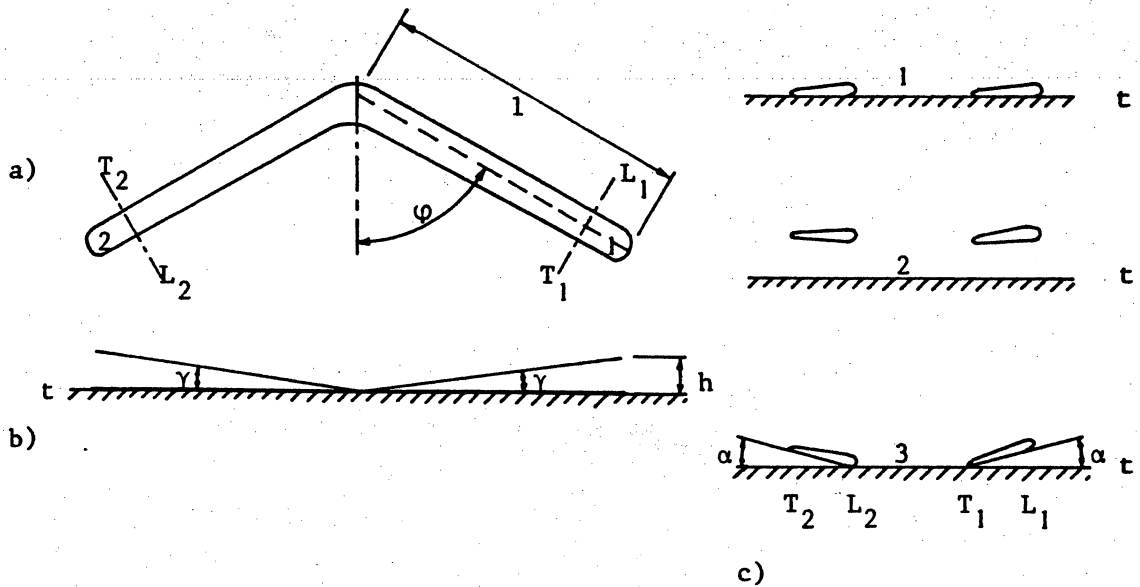


fig. 34.1. Dihedral  $\gamma$  obtained by kinking a plane boomerang at its elbow.  
 a) Planform of original boomerang resting on a table.  $l$  = length of arms, CM = centre of mass,  $L_1, L_2$  = leading edges,  $T_1, T_2$  = trailing edges.  
 b) Edge-on view, showing dihedral  $\gamma$ . Wing tips are raised at a height  $h$  above the table.  
 c) Cross sections  $L_1T_1$  and  $L_2T_2$ ,  $t$  = table. 1 : Original position, 2 : After kinking, raised above the table, 3 : Kinked boomerang resting on table again.

Let us consider an idealized example (see fig. 34.1). Suppose a boomerang rests on a flat table. The boomerang is nearly plane, has a symmetrical planform, and consists of two straight, narrow arms of length  $l$ , which include an angle  $2\phi$ . The arms are connected by a hinge at the boomerang's elbow, so that they can rotate with respect to each other about the line at which the boomerang's plane of symmetry intersects the table. If the hinge in the elbow is kept in position on the table and each arm rotates upward over an angle  $\gamma$ , the tips of the arms will be raised by a distance  $h = l \sin \phi \sin \gamma$  above the table. If the hinge is

fixed, with epoxy say, in this position, we have obtained a boomerang with a dihedral angle  $\gamma$ . Note that the boomerang's centre of mass is also raised above the table and that the boomerang's principal axis of inertia is not perpendicular to the table anymore. However, let go of the hinge, and our new boomerang will rest on the table with the trailing edge of its arm nr. 1 ( $T_1$ ) and the leading edge of its arm nr. 2 ( $L_2$ ) touching the table. Note that, in this position, the boomerang's main axis of inertia is perpendicular to the table again. The leading edge of arm nr. 1 ( $L_1$ ) and the trailing edge of arm nr. 2 ( $T_2$ ) are raised above the table. This means that our new boomerang differs from the original one by a change in the geometrical angle of incidence of its arms. For arm nr. 1 this angle is increased by  $\alpha$ , for arm nr. 2 it is decreased by  $\alpha$ . The relation between  $\alpha$  and  $\gamma$  is given by:

$$\sin\gamma = \sin\alpha \cos\varphi \quad (34.1)$$

For example, if  $\gamma$  and  $\alpha$  are small angles, and the boomerang's arms include an angle  $2\varphi = 90^\circ$ , we have  $\gamma \approx 0.7\alpha$  and  $\alpha \approx 1.4\gamma$ . For  $2\varphi = 120^\circ$ :  $\gamma \approx 0.5\alpha$ ,  $\alpha \approx 2\gamma$ .

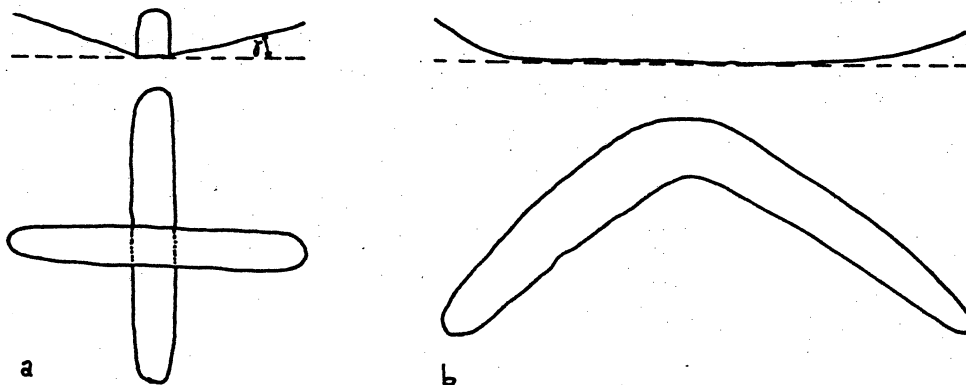


fig. 34.2 a) Cross boomerang with dihedral  $\gamma$ .

b) Boomerang with wing tips bent upward.

This exposition shows that a two-armed boomerang having a clear-cut dihedral behaves as a boomerang without dihedral, but having arms with changed angles of incidence. However, a cross-boomerang, whose arms are rotated upward over an angle  $\gamma$ , is a quite different case (see fig. 34.2a). The above line of reasoning does not apply to boomerangs with arms whose local spanwise directions deviate from the boomerang's plane

of rotation (= plane perpendicular to principal axis of inertia). Although we did not make calculations for model boomerangs of this kind, such cases can be very well dealt with in our winglet model (see Part II, §2). In the practice of boomerang making it may be interesting to employ the upward or downward bending of the wing tips as one of the factors in the design (see fig. 34.2b). On the other hand, such deformations may be undesirable when they are caused by accidental warp. The upward bend of the tips will nearly always result in (at least a slight) change of the boomerang arms' angles of incidence, as discussed above. However, apart from this effect, it is plausible that the lift on each arm is increased when the arm points forward in the boomerang's flight, and decreased when the arm points backward. This would result in a higher value for the pitching torque  $T_y$ , which in turn would cause the boomerang to lie down faster by precession.

Strictly speaking, the model boomerangs for which flight paths are shown in fig. 34.3 do not have a dihedral. The parameter varied is  $\alpha_{ot}$ , the geometrical angle of incidence of the profile near the tip of a boomerang arm. If  $\alpha_{ot}$  is increased for one arm, it is decreased by the same amount for the other arm. The corresponding angle at the root of the arm,  $\alpha_{or}$ , is kept constant. (For a definition of these parameters, see Part II, §22.) The model boomerangs differ from each other only in  $\alpha_{ot}$ , otherwise they are identical with boomerang 195.1 (see Part II, table 32.1). Values of  $\alpha_{ot}$  for the three boomerangs considered are listed in table 34.1. Roughly speaking, if boomerang 195.1 is given a positive dihedral of about  $2^\circ$ , one would obtain a boomerang more or less resembling the 262.1, and if boomerang 195.1 is given a negative dihedral of about  $2^\circ$ , one would obtain a boomerang more or less resembling the 263.1. Strictly speaking, one obtains boomerang 262.1 from boomerang 195.1 by giving arm nr. 1 a positive twist of  $3^\circ$ , and arm nr. 2 a negative twist of  $3^\circ$ . For boomerang 263.1 the converse is true.

The effect of the chosen variations in  $\alpha_{ot}$  on the aerodynamic forces are illustrated by table 34.2, which lists some data for  $\Psi = 10^\circ$ ,  $U = 1$ . *Only  $T_{1y}$  varies, the five other components (including those not listed here) remain essentially constant.* This remarkable phenomenon can be observed in many other computed cases, in which the angle of incidence

boomerang nr.	arm nr. 1		arm nr. 2	
	normal	reversed	normal	reversed
263.1	+2.0°	+2.0°	+5.0°	-1.0°
195.1	+5.0°	-1.0°	+2.0°	+2.0°
262.1	+8.0°	-4.0°	-1.0°	+5.0°

Table 34.1.  $\alpha_{ot}$  for the model boomerangs.

is increased for one arm and decreased by the same amount for the other arm. The net result of such a modification appears to be a shift of a part of the average lift forward or backward over a distance proportional to the difference in excentricity of the boomerang arms concerned. The magnitude of this effect can also be calculated by means of the simple model of [Hess, 1968], in which the induced velocity of the air is neglected. It is remarkable that the results of this model closely agree with those of the winglet model. For an explanation of the effect see [Hess, 1968, p. 131] and also Part I, §17. (Excentricity: Part II, §20).

bnr	$F_{1z}$	$T_{1x}$	$T_{1y}$	$\frac{T_{1x}}{F_{1z}}$	$\frac{T_{1y}}{F_{1z}}$	$\frac{T_{1y}}{T_{1x}}$
263.1	.1660	.0404	.0102	.244	.061	.252
195.1	.1644	.0401	.0131	.244	.080	.327
262.1	.1622	.0399	.0161	.246	.099	.403

Table 34.2. Some aerodynamic values at  $\Psi = 10^\circ$ ,  $U = 1$ .

Figure 34.3a,b and fig. 33.1a show flight paths computed for the three boomerangs with the following initial conditions:

$$f_o = 11 \text{ rev/s}, V_o = 27 \text{ m/s}, \Psi_o = 0^\circ,$$

$$\phi_o = 90^\circ, \varphi_o = 0^\circ, \psi_o = -20^\circ,$$

$$X_o = 0 \text{ m}, Y_o = 0 \text{ m}, Z_o = 1.8 \text{ m},$$

no wind

Some values for these flights are listed in table 34.3.

Obviously, a main difference between the three flight paths concerns the maximum elevation ( $Z_2$ ). Boomerang 263.1 remains relatively low, whereas boomerang 262.1 attains a considerably greater height. This was

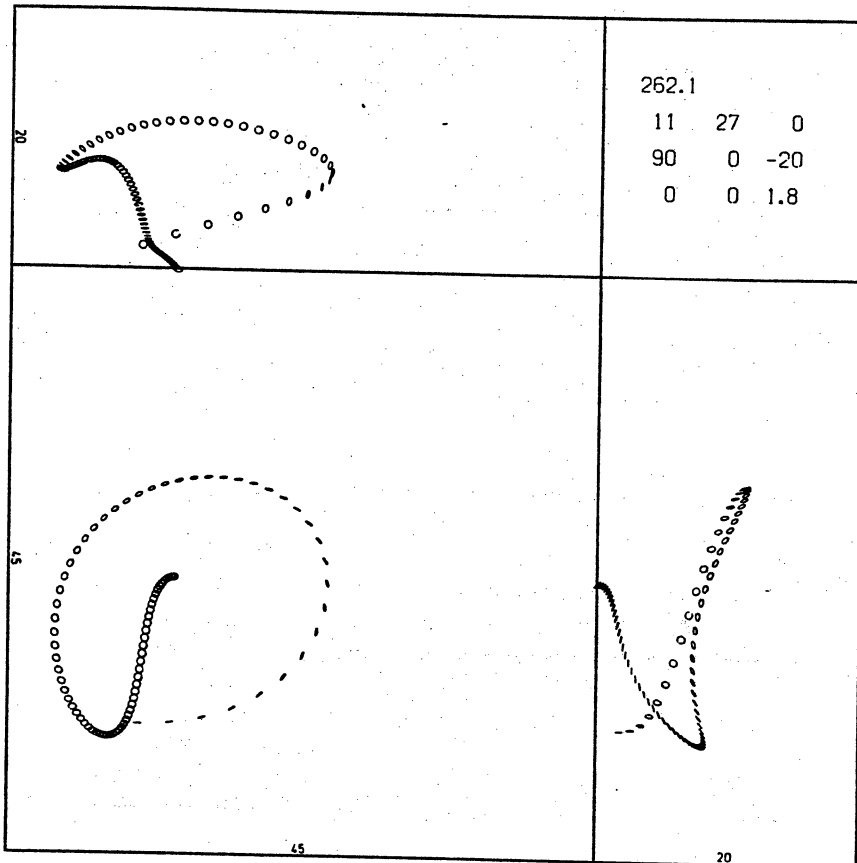


fig. 34.3a

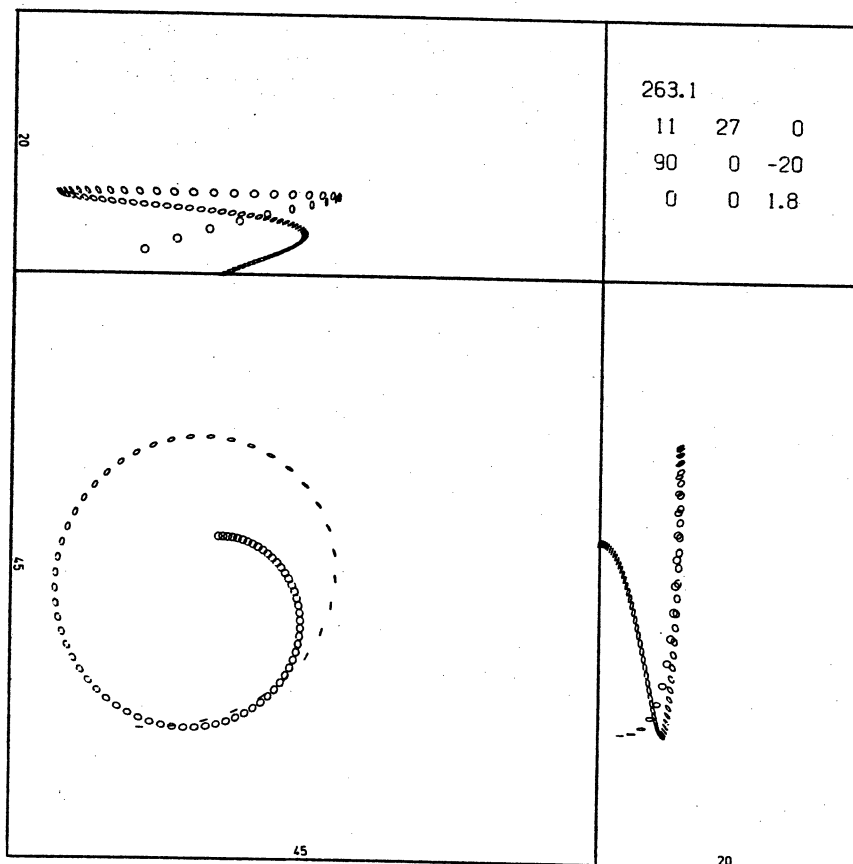


fig. 34.3b

bnr	t	P	n	D	Z <sub>2</sub>	D <sub>2</sub>	D <sub>1</sub>	f <sub>2</sub>	f <sub>1</sub>	V <sub>1</sub>	ψ <sub>2</sub>	U <sub>1</sub>
263.1	8.8	97.0	86.1	16.0	6.3	23.3	0.8	11.0	9.4	3.9	29.2	.22
195.1	10.2	92.3	99.1	12.9	9.4	22.3	1.2	11.0	9.4	1.7	85.7	.09
262.1	8.6	80.9	78.1	11.6	11.4	20.7	0.9	11.0	8.5	2.8	43.9	.17

Table 34.3. Some values of the flights of fig. 34.3 and fig. 33.1a.

to be expected on the basis of the differences in the torque  $T_y$ : boomerang 262.1 lies down faster than boomerang 263.1 does. Table 34.4 lists some values at  $t=1$  sec.

bnr	t sec	f rev/s	V m/s	U	ψ degr	θ degr	φ degr	ψ degr
all	0	11.0	27.0	1.31	0.0	90.0	0.0	-20.0
263.1	1.0	10.3	20.0	1.04	9.6	80.1	108.2	- 3.6
195.1	1.0	10.3	19.1	0.99	10.8	77.5	113.1	-12.8
262.1	1.0	9.9	17.7	0.95	13.2	77.4	121.0	-22.2

Table 34.4. Some values for the flights at  $t=1$  sec.

A qualitatively similar influence of variations in  $T_y$  on the shape of boomerang flight paths was shown in [Hess, 1968, p. 134] (there the parameter  $\beta$  equals  $\arctg(T_{1y}/T_{1x})$ ).